Supporting Information

Twist, Grind, Translocate: Pepper-Mill Dynamics of MSPA protein pore during ssDNA Transport†

Priya Dey, Brandon Meza-Gonz´alez, Ganesh N. Pandian and Daniel M. Packwood*

S1. Secondary Structure Analysis of MSPA protein

(a)

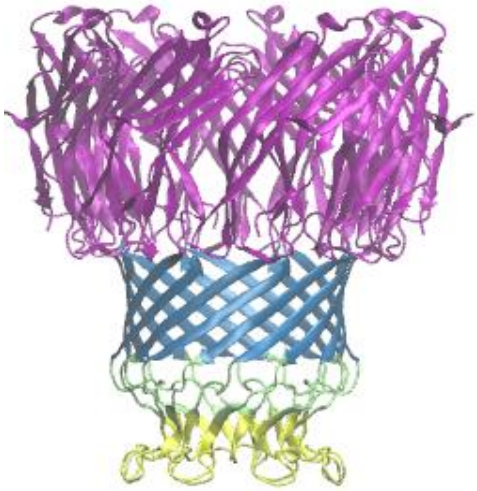

(b)

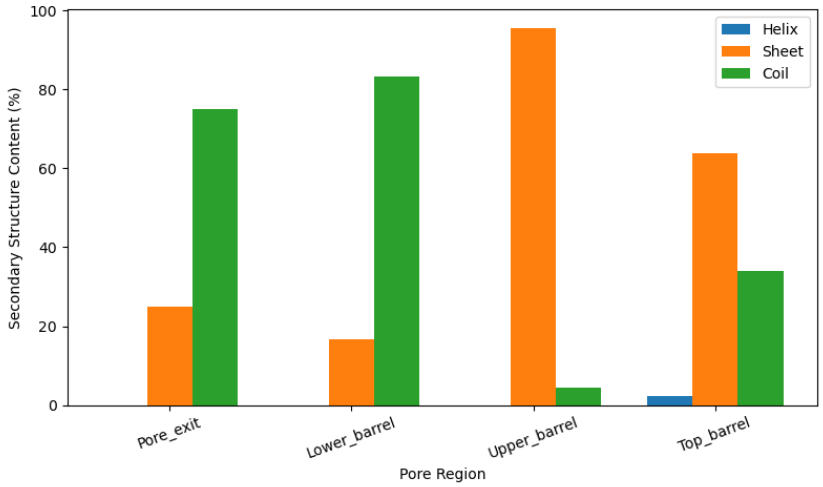

(c)

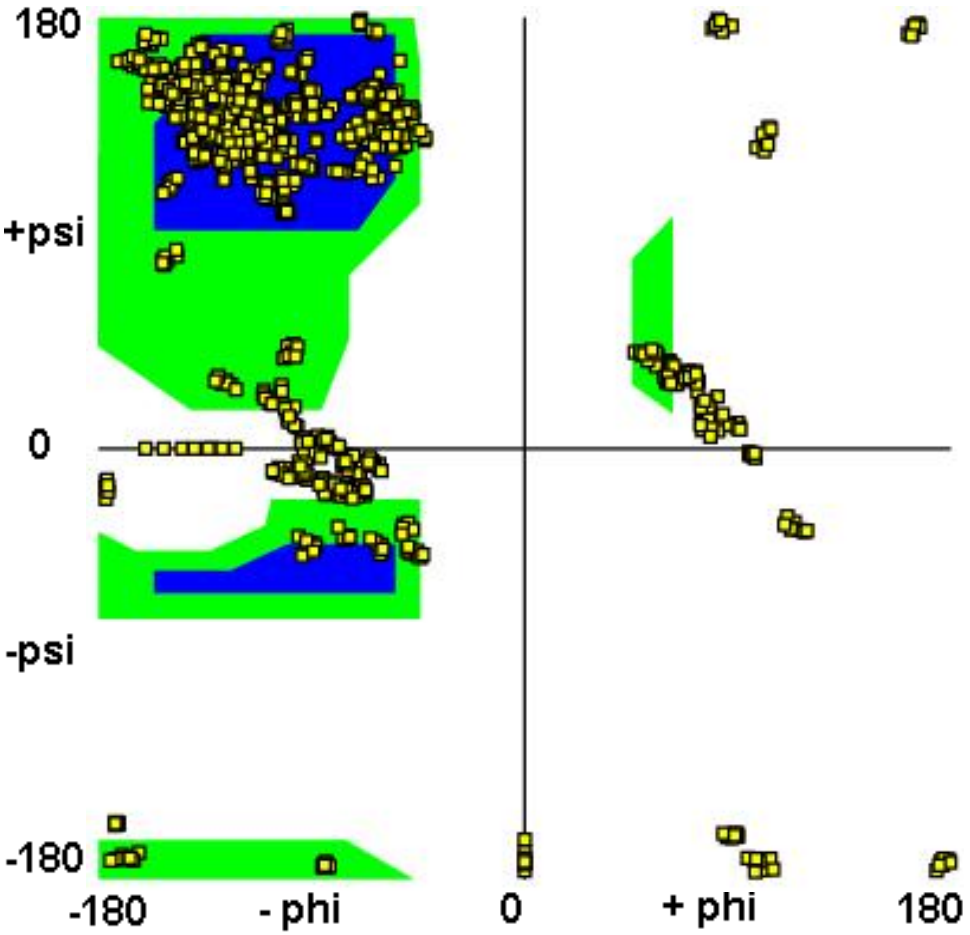

Figure S1: [a] New Cartoon representation, [b] Secondary Structure content of the pore parts, and [c] Ramachandran plot for the MSPA Protein.

S2. Graphical Representation of Simulation Box:

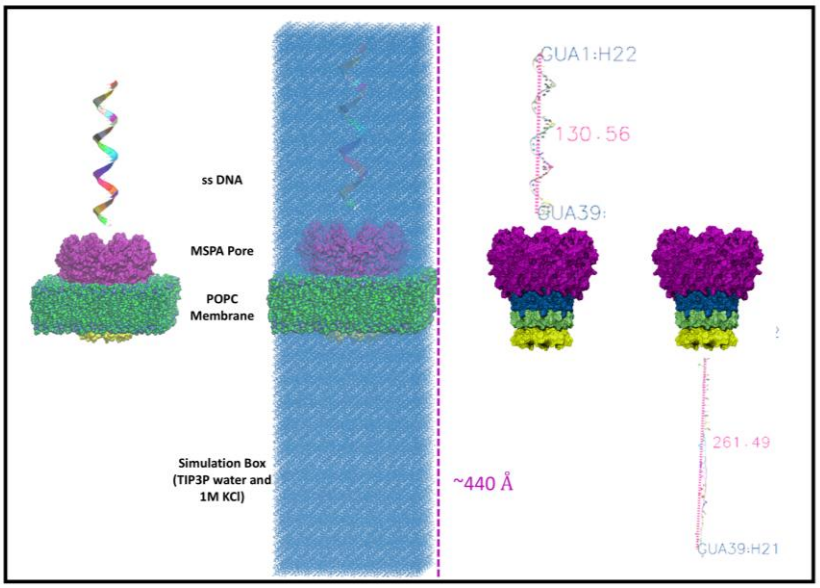

S3. Equilibration Prior to Steered Molecular Dynamics Simulations:

The system was equilibrated following the standard multi-stage CHARMM-GUI membrane equilibration protocol, consisting of six consecutive equilibration steps with gradually released restraints. The equilibration details are as follows:

Step Equi1: 125,000 steps × 1 fs = 125 ps (NVT, Langevin thermostat)

Step Equi2: 125,000 steps × 1 fs = 125 ps (NVT, Langevin thermostat)

Step Equi3: 125,000 steps × 1 fs = 125 ps (NPT, Nosé–Hoover thermostat)

Step Equi4: 250,000 steps × 2 fs = 500 ps (NPT)

Step Equi5: 250,000 steps × 2 fs = 500 ps (NPT)

Step Equi6: 250,000 steps × 2 fs = 500 ps (NPT)

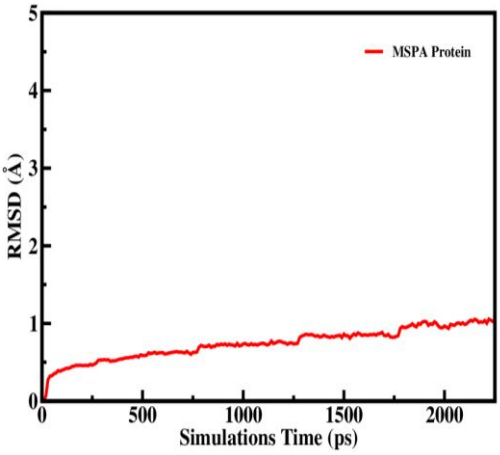

This results in a total equilibration time of approximately 1.875 ns prior to the production SMD simulations.

S4. The Cumulative Explained Variance

(a)

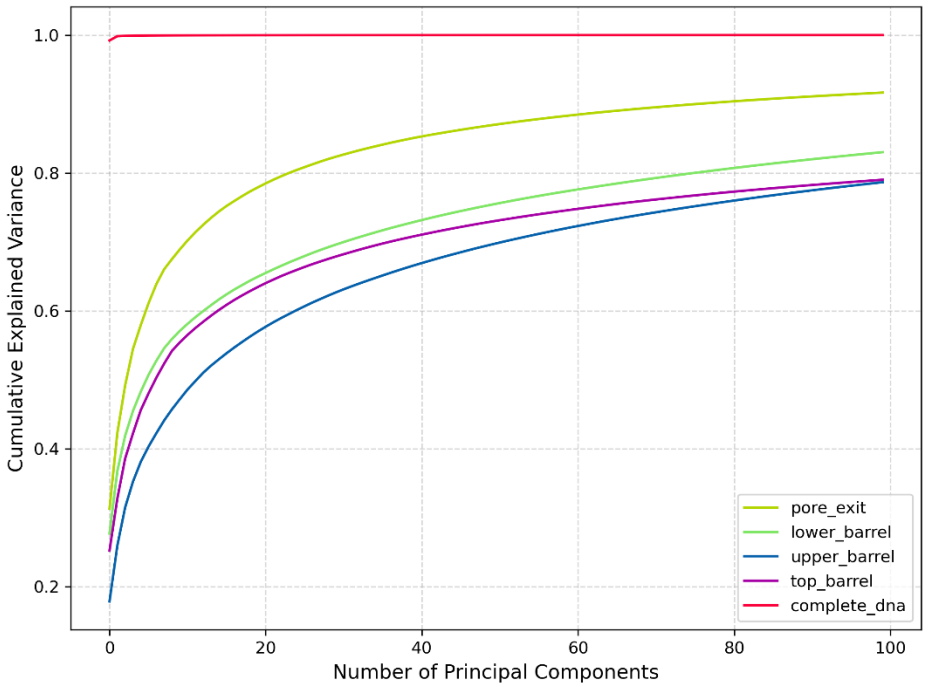

(b)

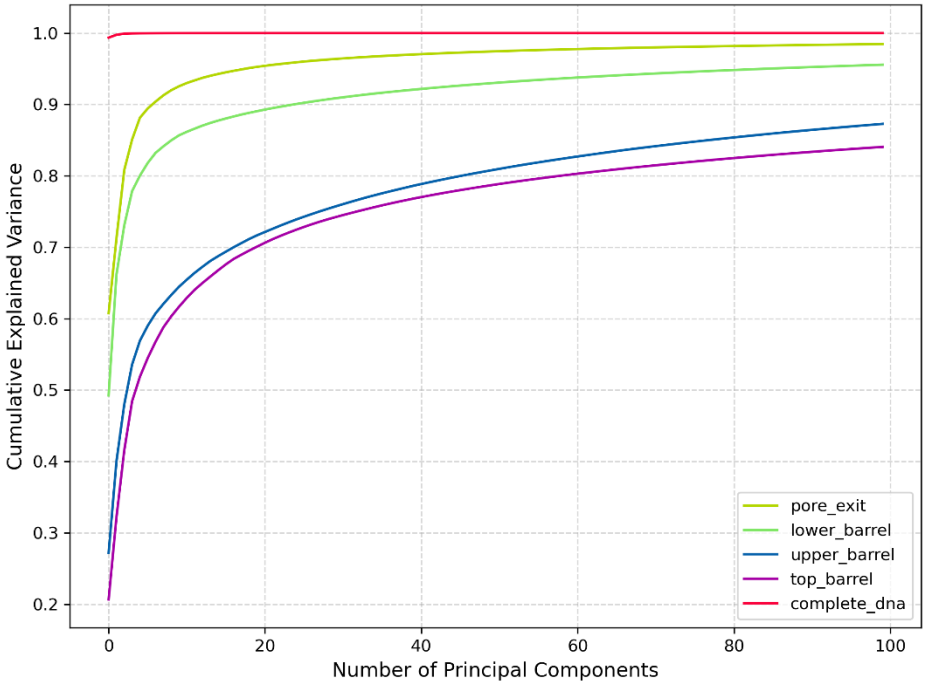

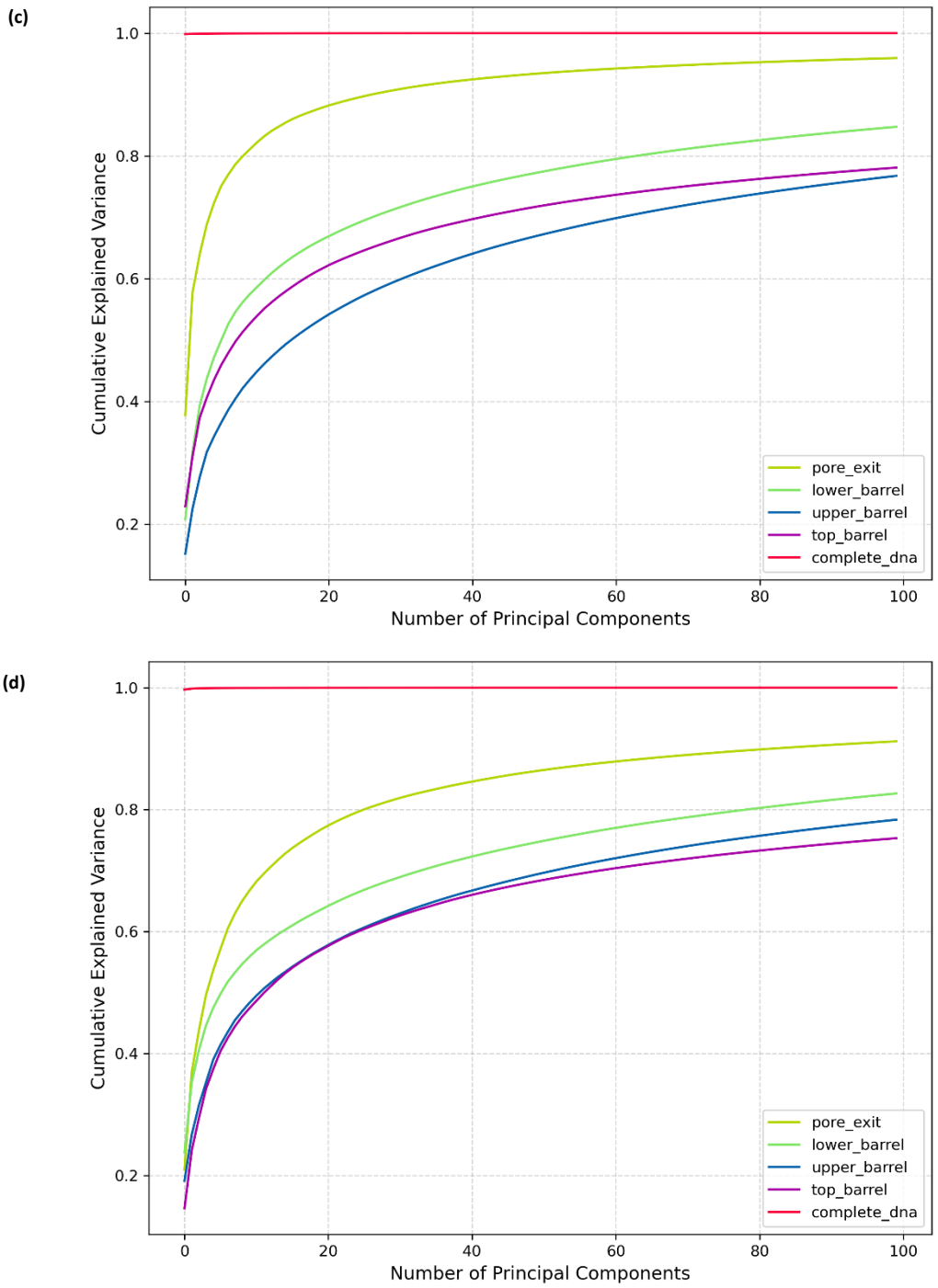

Figure S2: Cumulative explained variance of principal components for (a) polyA, (b) polyC, (c) polyG, and (d) polyT systems. Each plot shows the fraction of total variance captured as a function of the number of principal components, illustrating how many components are required to represent the dominant conformational dynamics of each system.

S5. DCC Analysis of MSPA Pore (In Absence of ssDNA Translocation)

The observed reverse twisting behavior between the upper and lower regions of the protein emerges specifically during ssDNA translocation. To verify whether this motion is an intrinsic property of the protein, we performed additional control simulations of the protein embedded in a lipid bilayer and solvated in a cuboidal water box, in the absence of ssDNA. DCC analysis of these simulations did not reveal any comparable twisting or counter-rotational motion. This indicates that the reverse twisting is not an inherent fluctuation of the protein but is instead induced by, and functionally coupled to, ssDNA translocation through the pore.

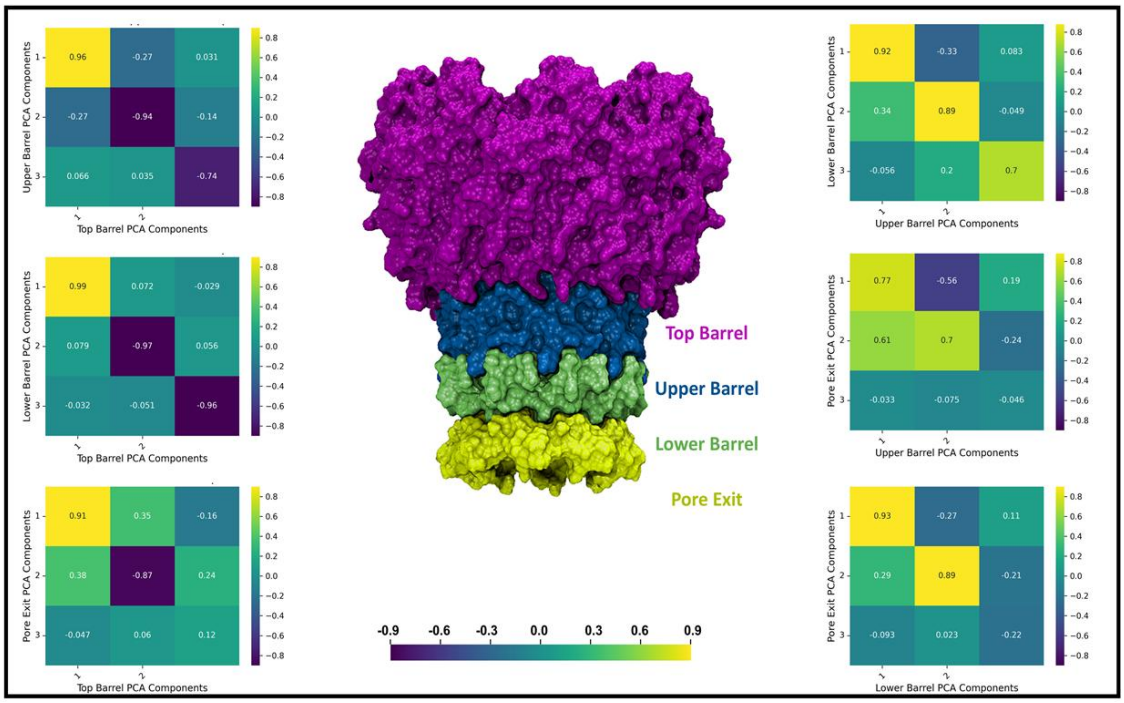

Figure S3: Dynamic cross-correlation (DCC) matrices between structural regions of the MSPA pore in the absence of ssDNA.

S6. Dynamic Cross Correlation Matrix

(a)

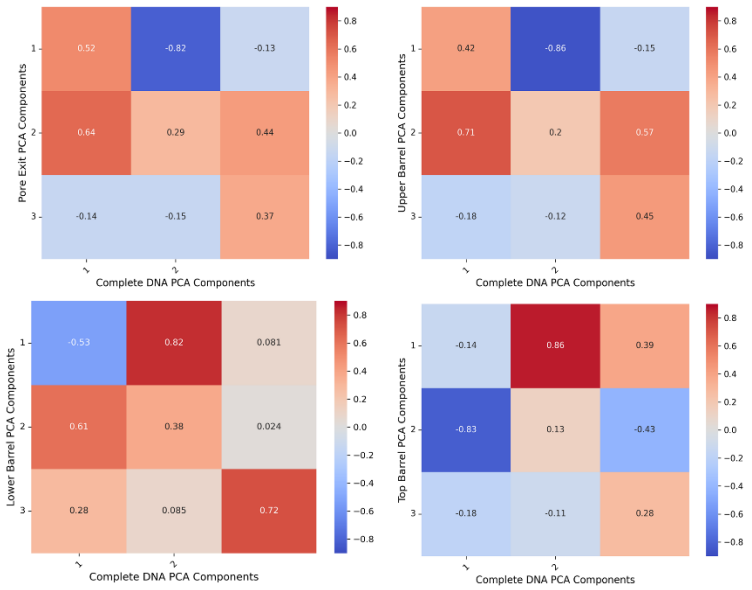

(b)

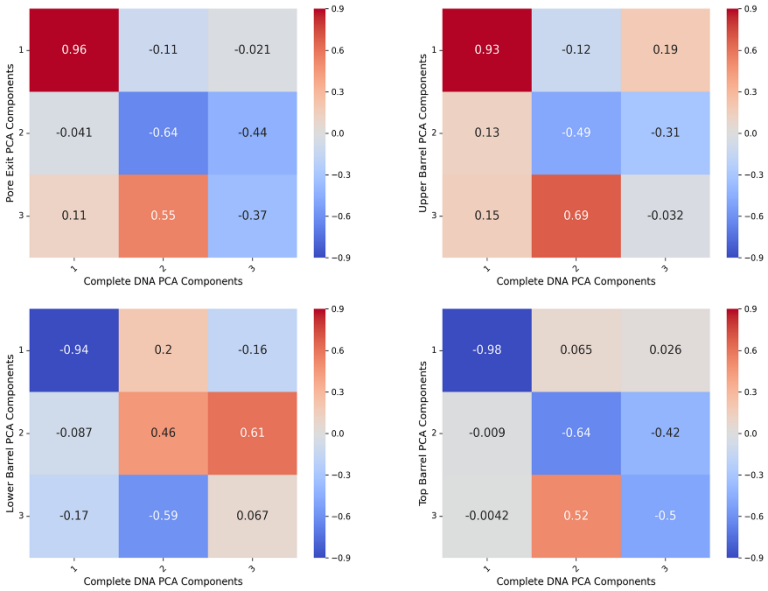

(c)

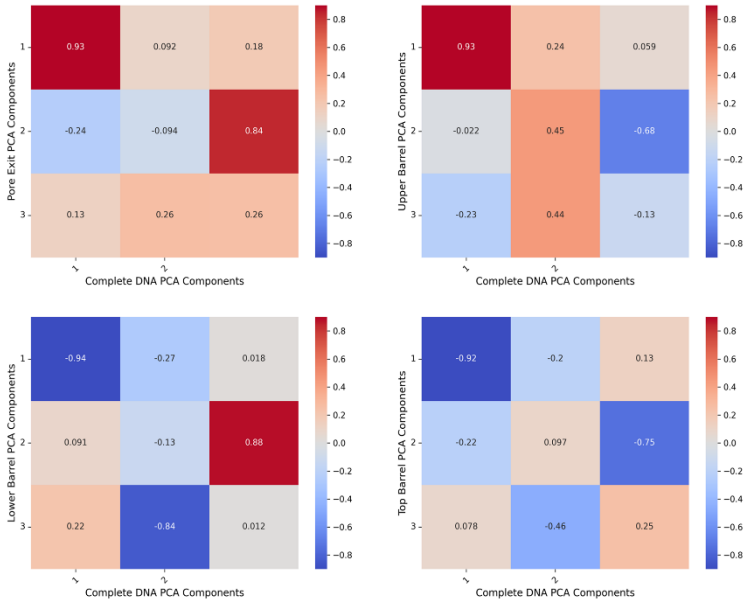

Figure S4: Dynamic cross-correlation (DCC) matrices of MSPA pore regions with the translocating ssDNA for (a) polyC, (b) polyG, and (c) polyT systems.

(a)

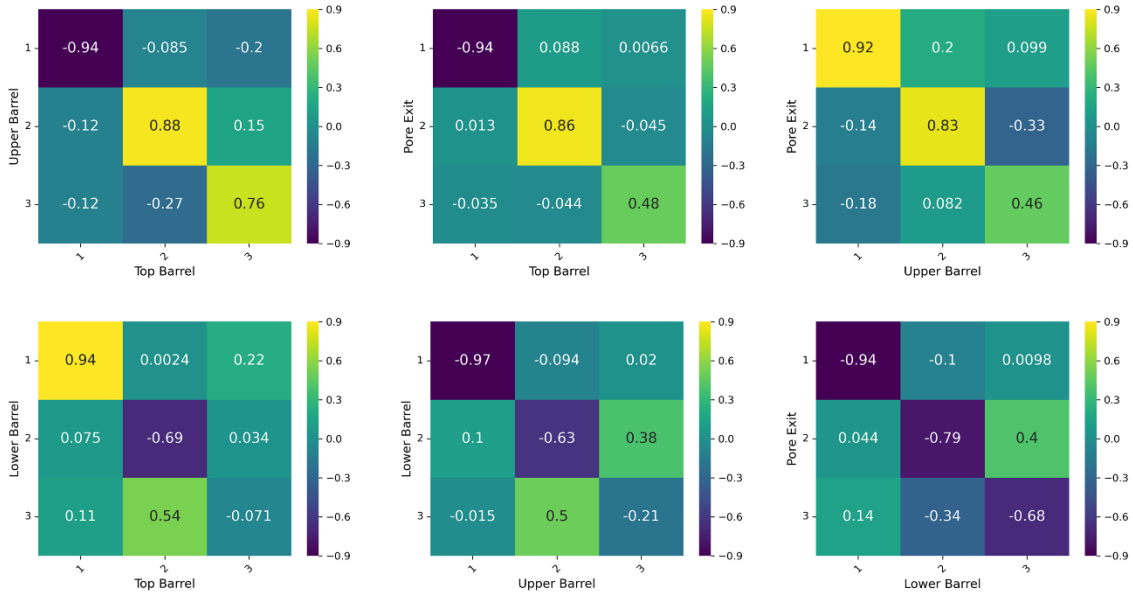

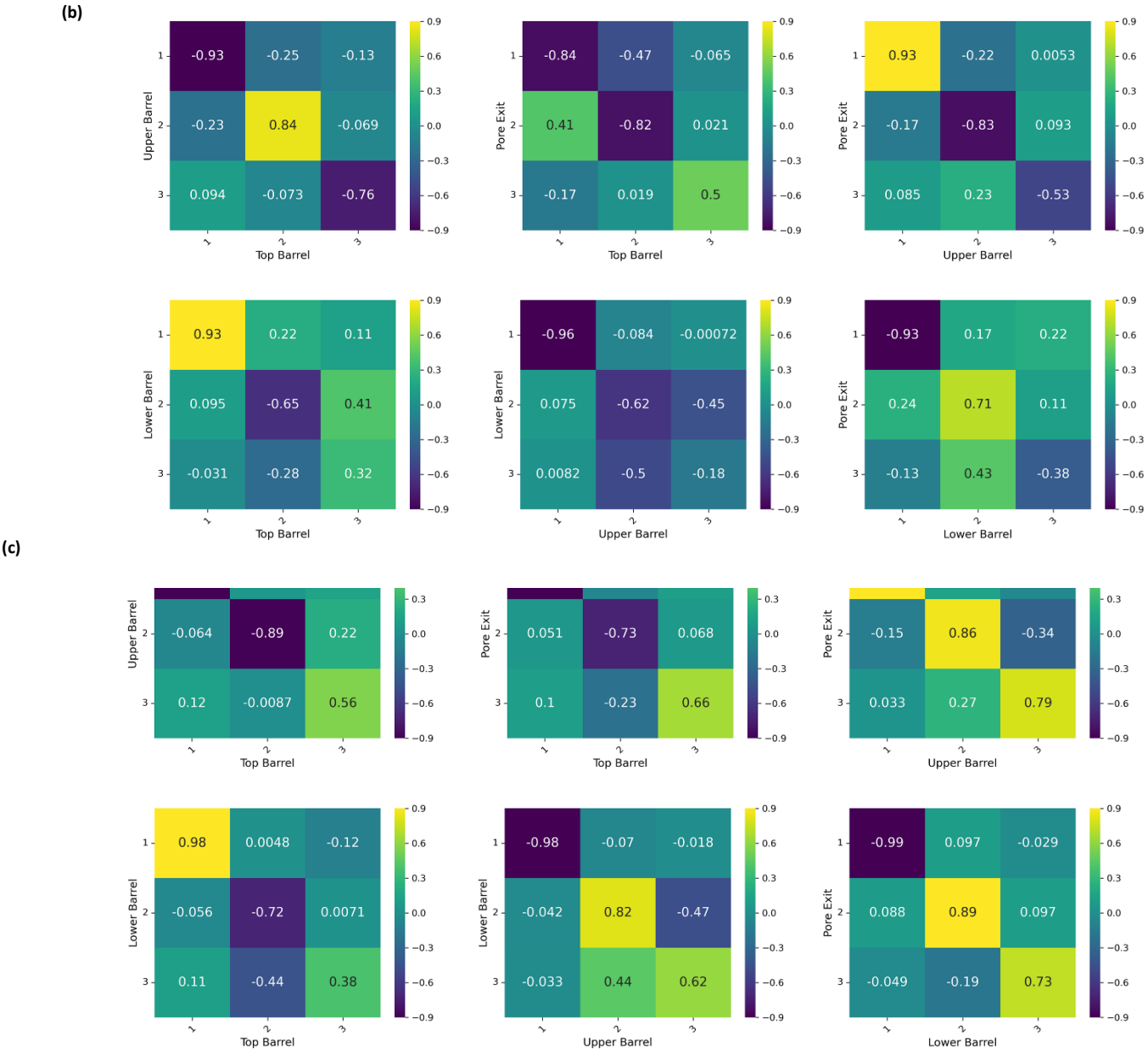

Figure S5: Dynamic cross-correlation (DCC) matrices between structural regions of the MSPA pore for (a) polyC, (b) polyG, and (c) polyU systems. Each matrix represents correlated (positive) and anti-correlated (negative) motions among the pore regions.

S7. Structural Analysis

S7.1: Root mean square deviation (RMSD)

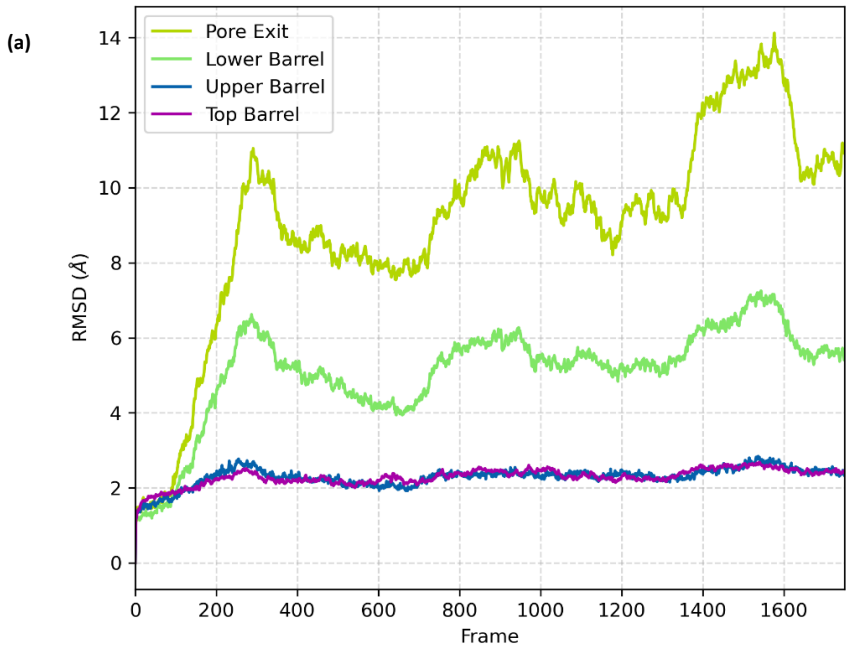

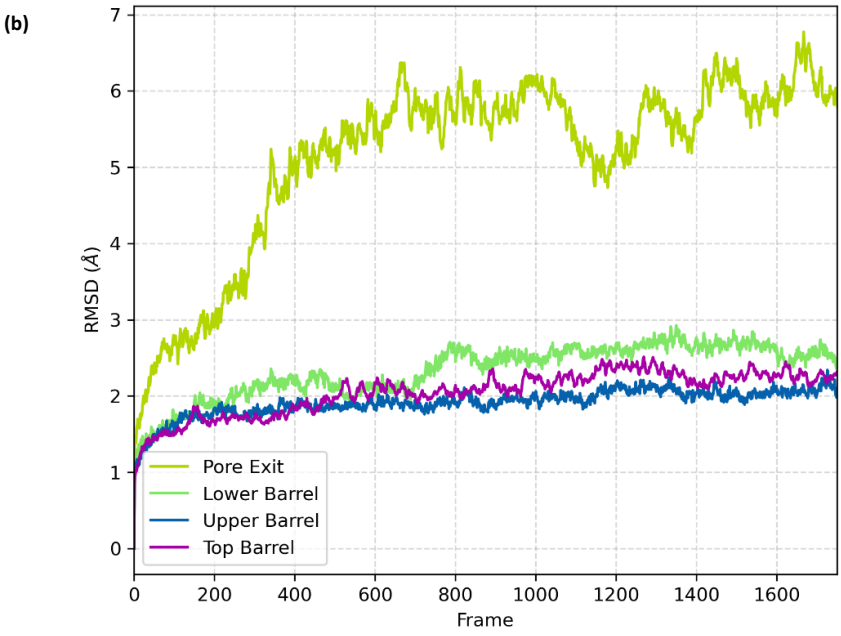

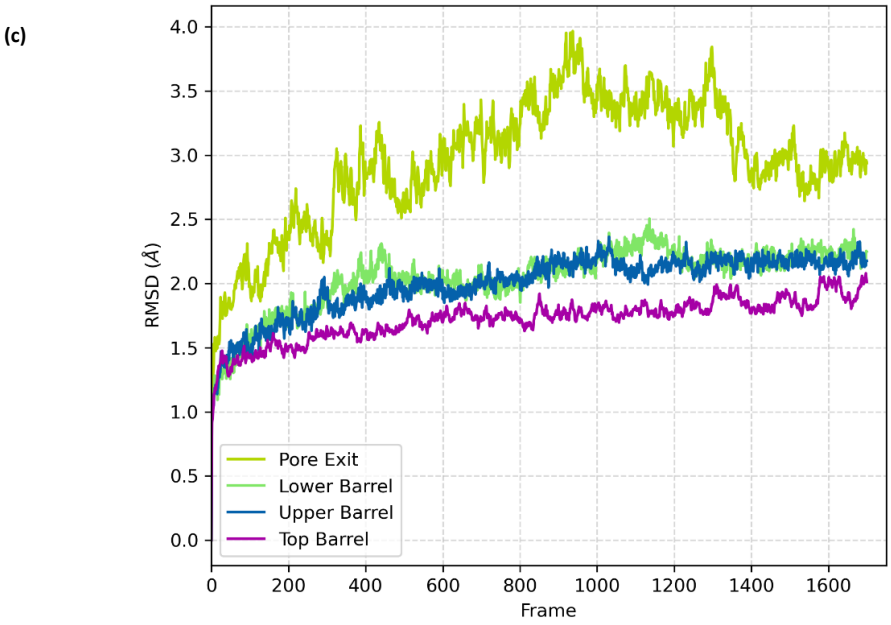

Figure S6: Root mean square deviation (RMSD) profiles for (a) polyC, (b) polyG, and (c) polyT systems. Each plot depicts the time evolution of RMSD, reflecting the structural stability and conformational fluctuations of the nucleotide systems during the simulation.

S7.2 Intermolecular Contacts

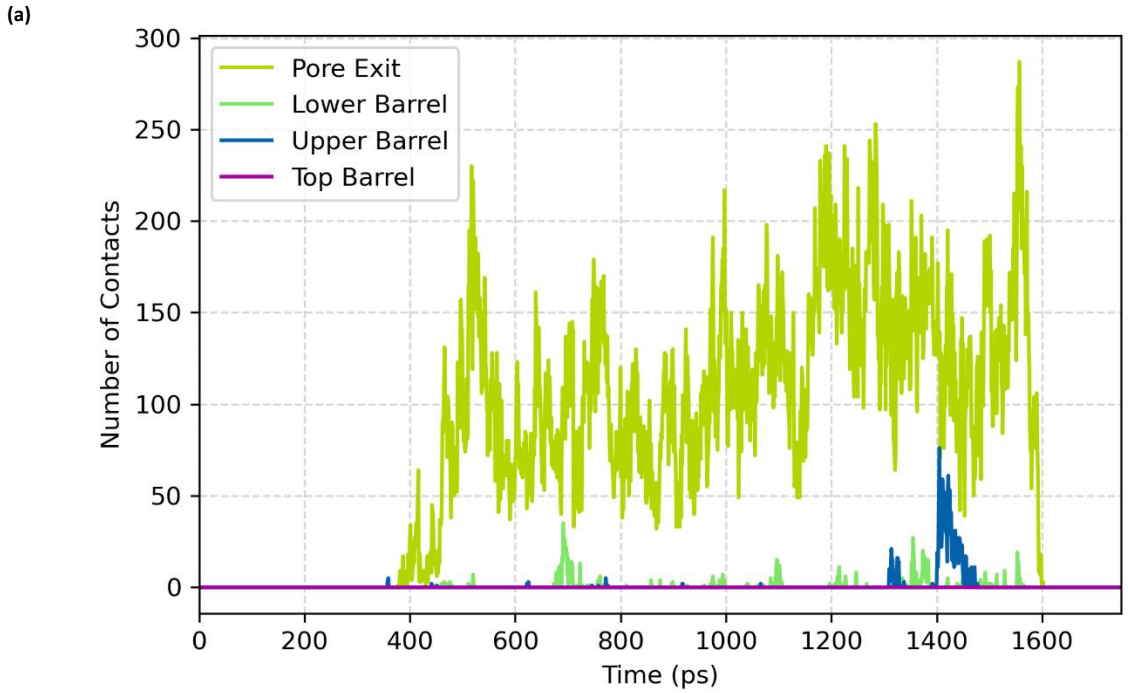

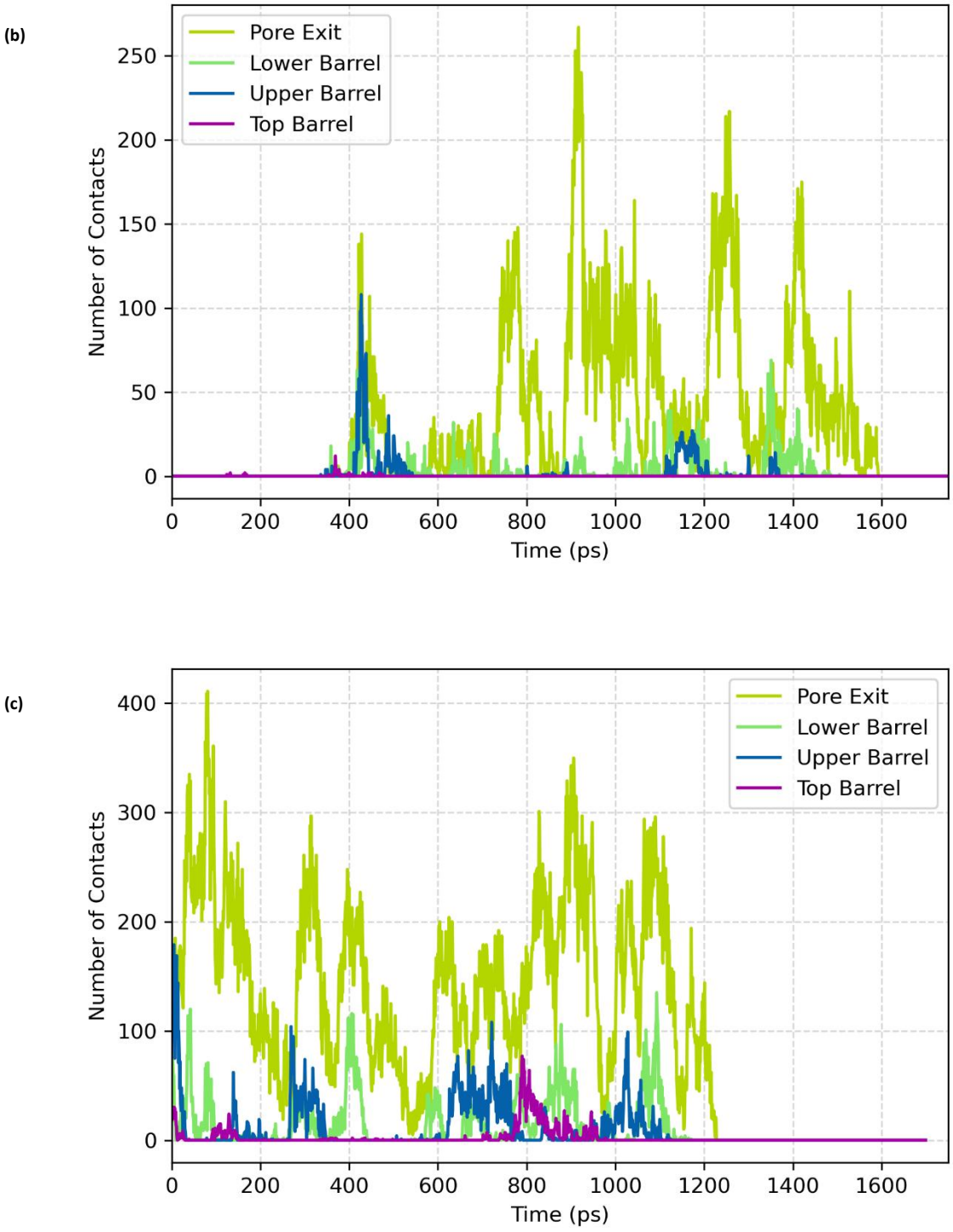

Figure S7: Number of intermolecular contacts for (a) polyC, (b) polyG, and (c) polyT systems. Each plot shows the variation in contact number over time, highlighting differences in molecular interactions and compactness among the nucleotide systems during the simulation.

S7.3. Root mean square fluctuation (RMSF)

(a)

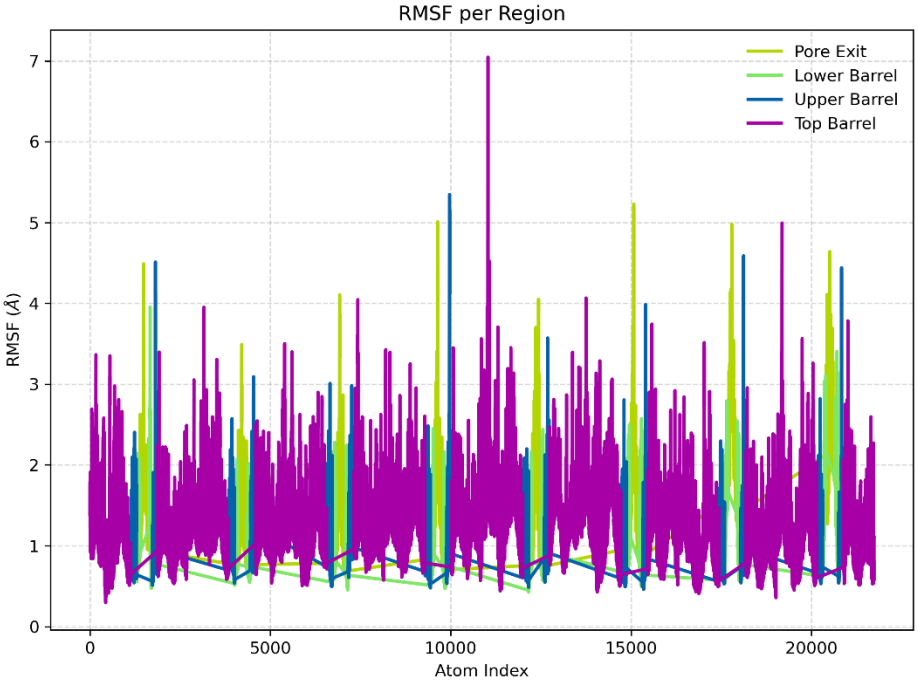

(b)

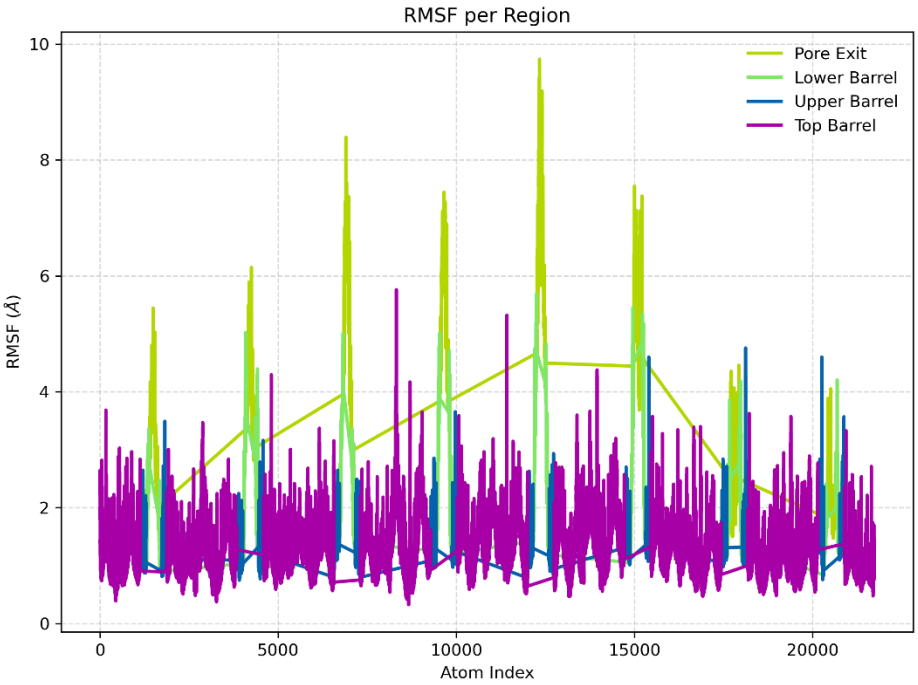

(c)

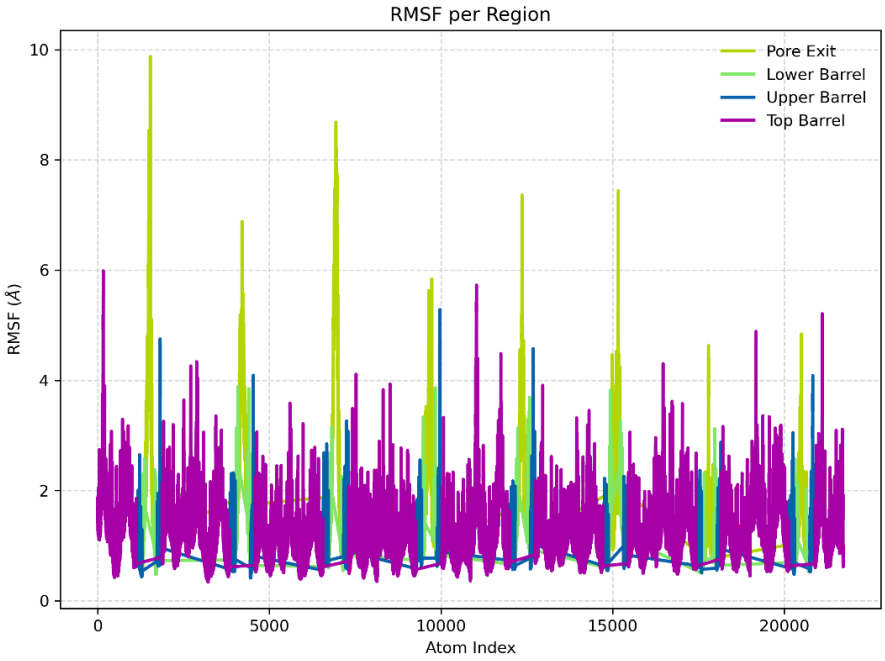

(d)

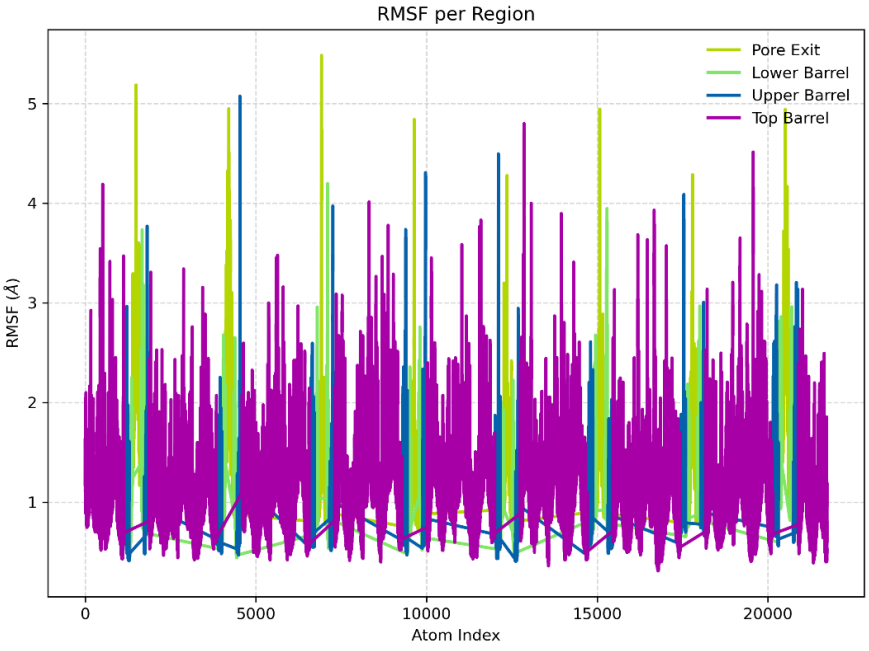

Figure S8: Root mean square fluctuation (RMSF) profiles for (a) polyA, (b) polyC, (c) polyG, and (d) polyT systems. Each plot represents the residue-wise atomic flexibility, indicating regions of high and low structural fluctuations across the nucleotide sequences during the simulation.

S7.4 Radius of Gyration

(a)

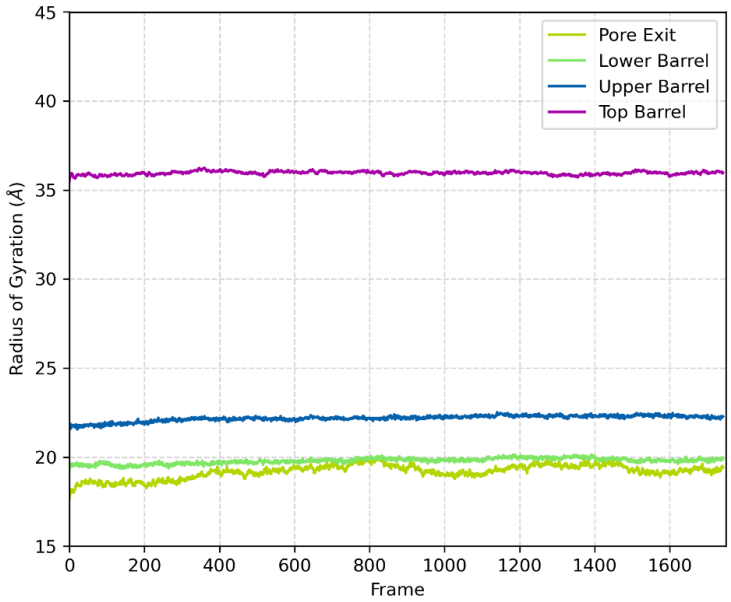

(b)

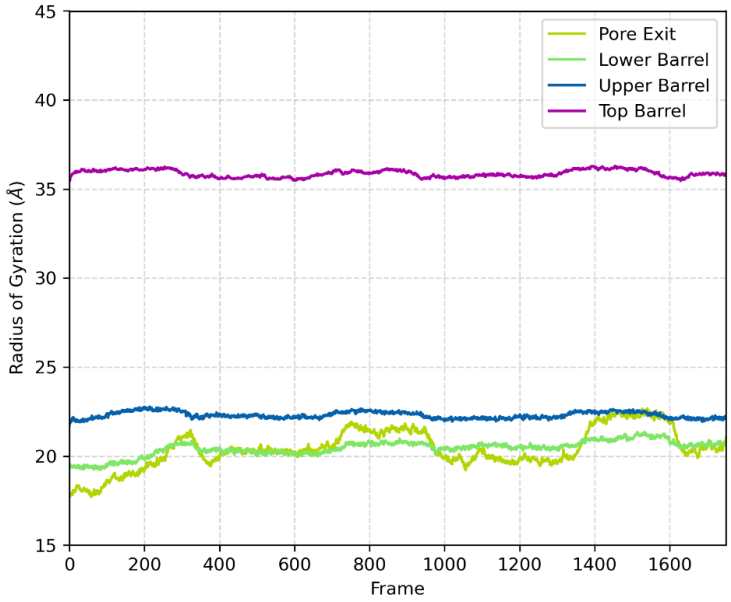

(c)

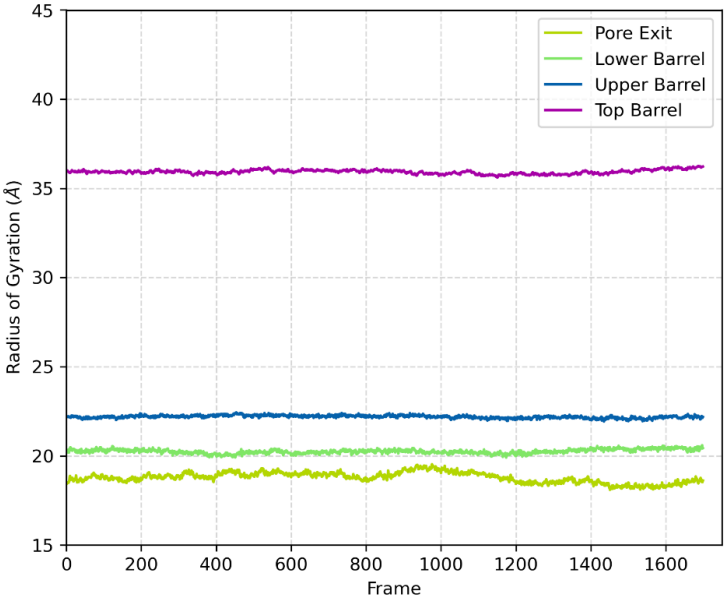

(d)

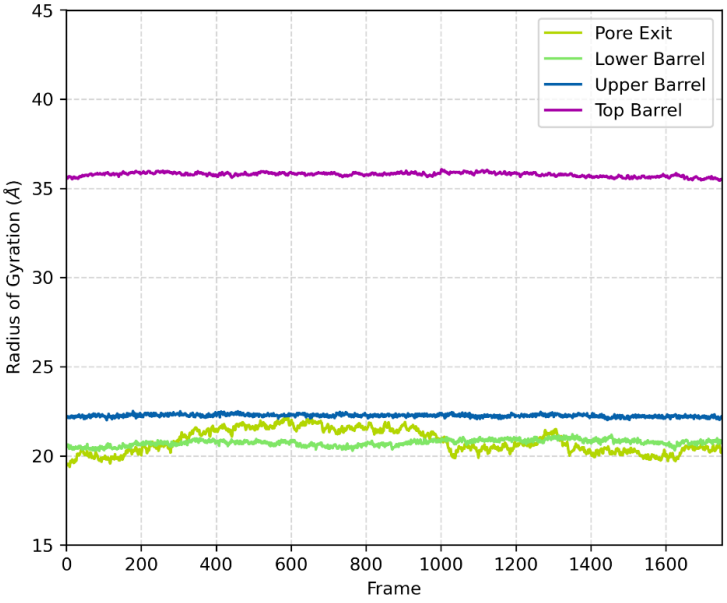

Figure S9. Radius of gyration (R_g) profiles for (a) polyA, (b) polyC, (c) polyG, and (d) polyT systems. Each plot shows the temporal evolution of R_g, reflecting the overall compactness and conformational stability of the nucleotide systems during the simulation.

S8. Residue-wise Contact formation between the Pore Exit residues and the ssDNA

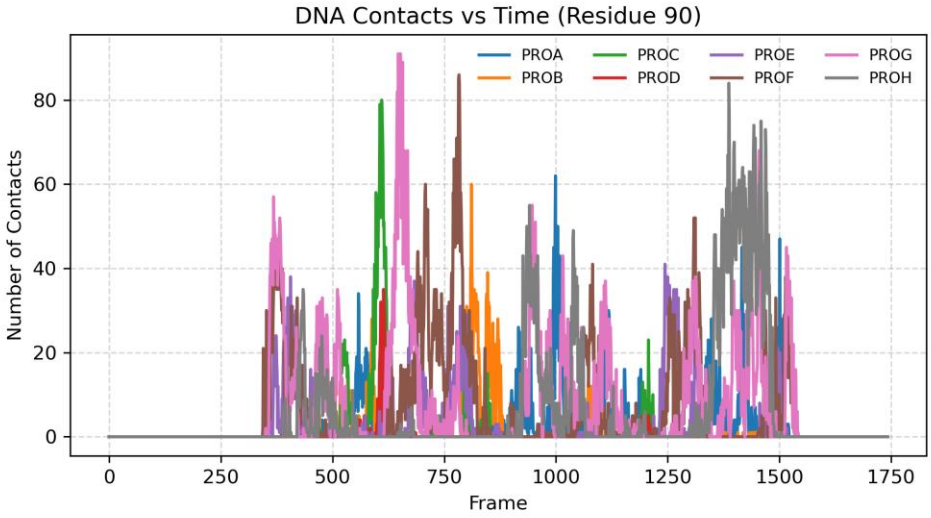

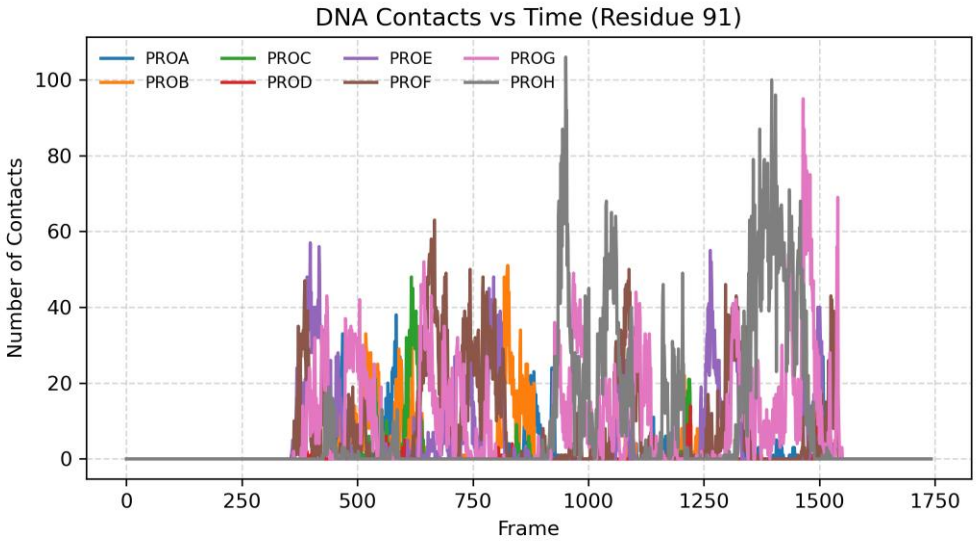

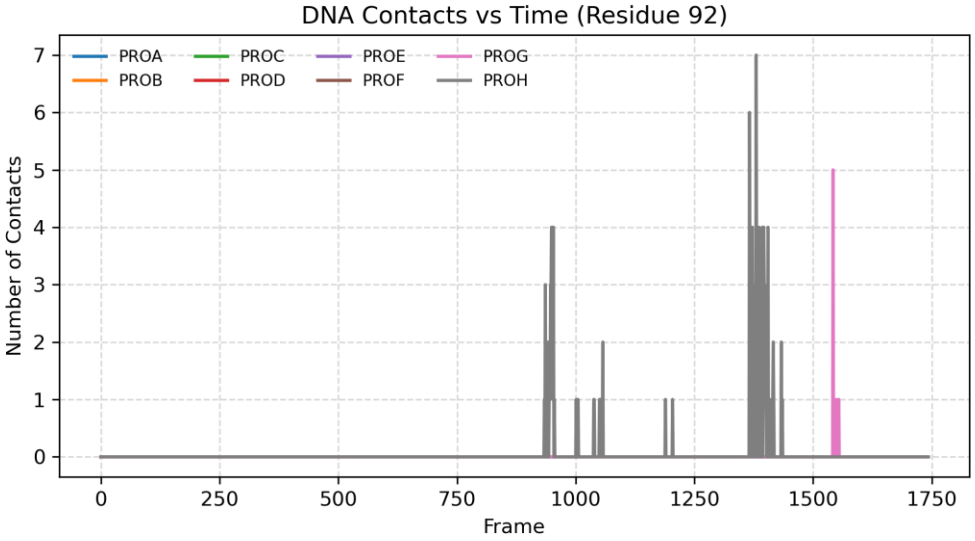
DNA Contacts vs Time (Residue 92)
PROA
PROB
PROC
PROD
PROE
PROF
PROG
PROH
Number of Contacts
Frame
0
1
2
3
4
5
6
7
0
250
500
750
1000
1250
1500
1750

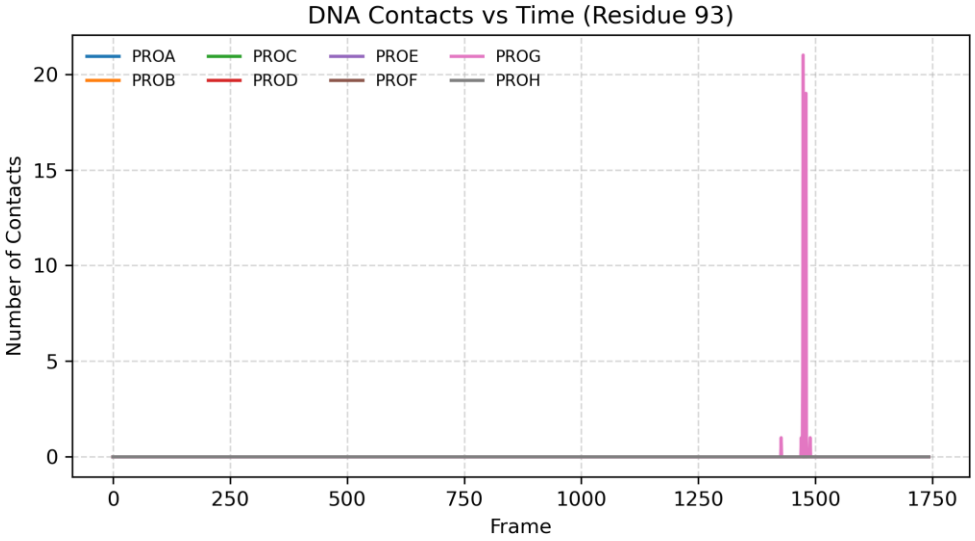
DNA Contacts vs Time (Residue 93)
PROA
PROB
PROC
PROD
PROE
PROF
PROG
PROH
Number of Contacts
Frame
0
5
10
15
20
0
250
500
750
1000
1250
1500
1750

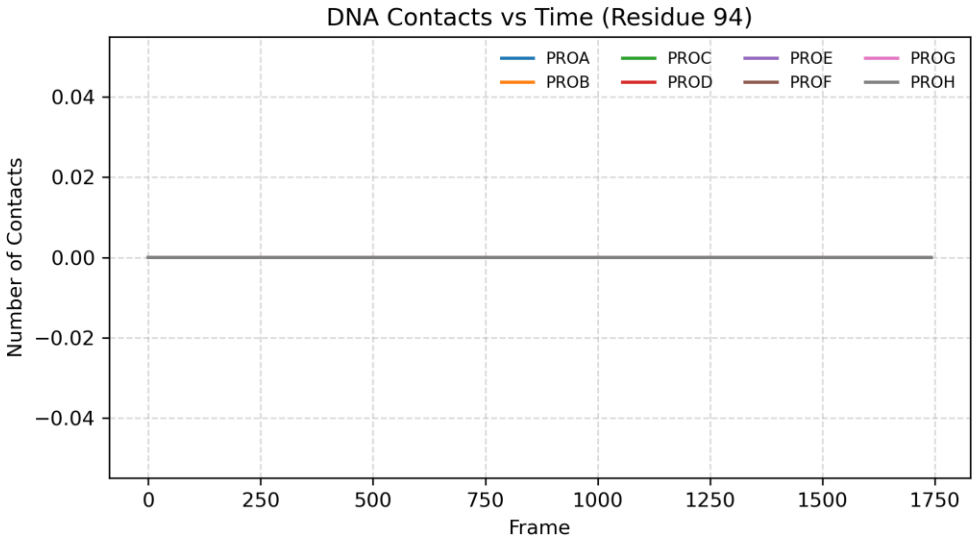
DNA Contacts vs Time (Residue 94)
PROA
PROB
PROC
PROD
PROE
PROF
PROG
PROH
Number of Contacts
0.04
0.02
0.00
−0.02
−0.04
0
250
500
750
1000
1250
1500
1750
Frame

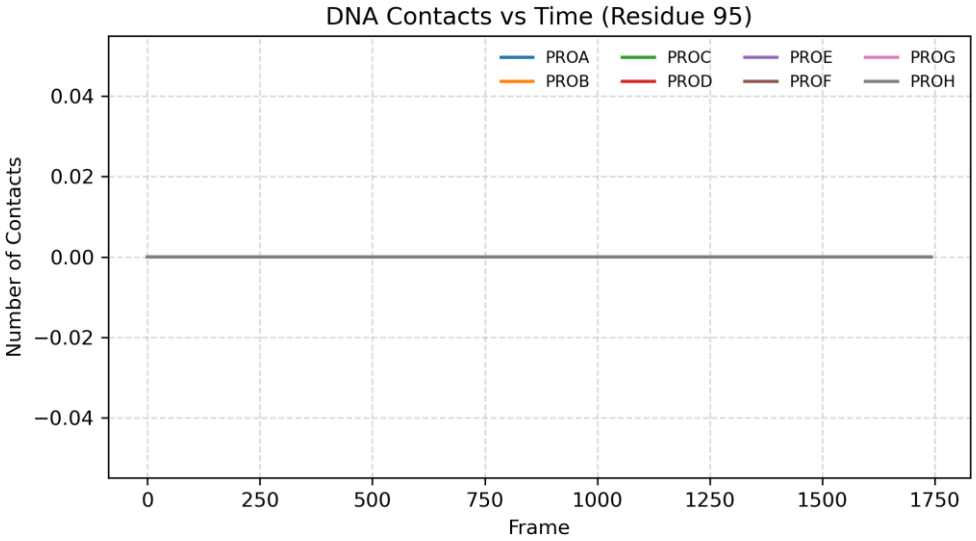
DNA Contacts vs Time (Residue 95)
PROA
PROB
PROC
PROD
PROE
PROF
PROG
PROH
Number of Contacts
0.04
0.02
0.00
−0.02
−0.04
0
250
500
750
1000
1250
1500
1750
Frame

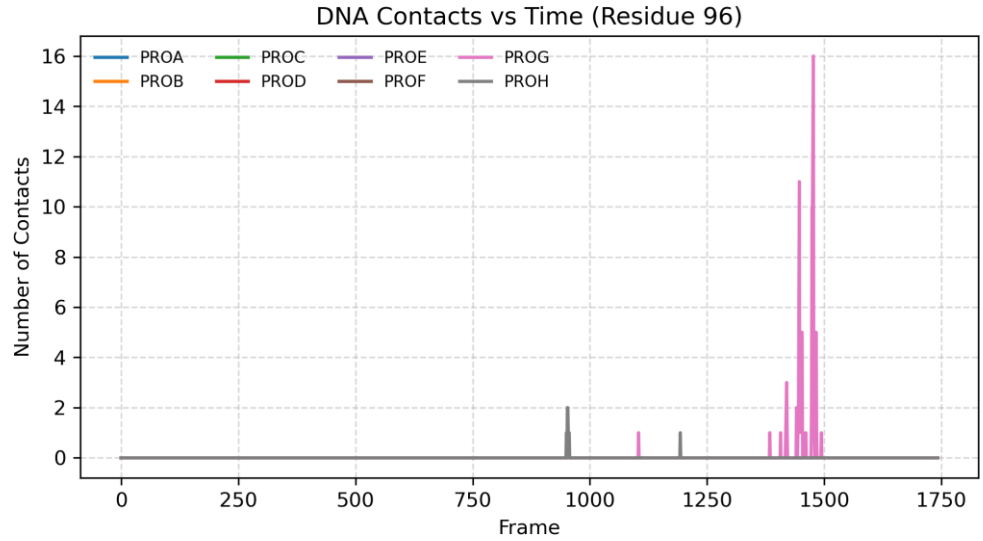
DNA Contacts vs Time (Residue 96)
PROA
PROB
PROC
PROD
PROE
PROF
PROG
PROH
Number of Contacts
16
14
12
10
8
6
4
2
0
0
250
500
750
1000
1250
1500
1750
Frame

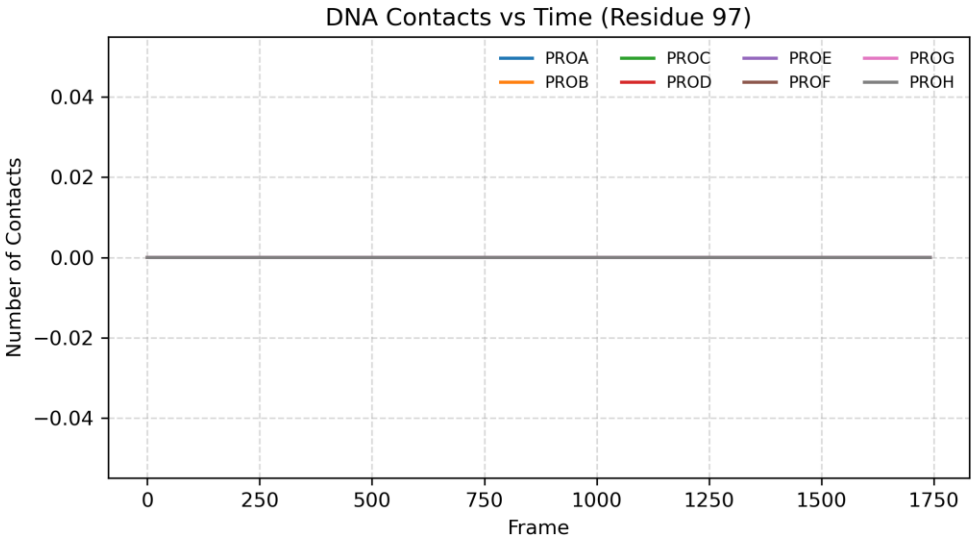
DNA Contacts vs Time (Residue 97)
PROA
PROB
PROC
PROD
PROE
PROF
PROG
PROH
Number of Contacts
0.04
0.02
0.00
−0.02
−0.04
0
250
500
750
1000
1250
1500
1750
Frame

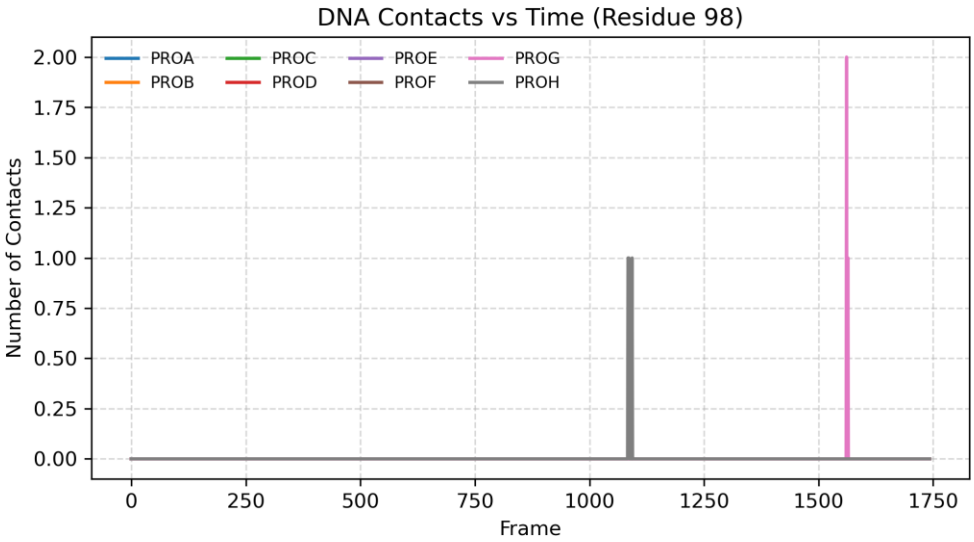
DNA Contacts vs Time (Residue 98)
PROA
PROB
PROC
PROD
PROE
PROF
PROG
PROH
Number of Contacts
2.00
1.75
1.50
1.25
1.00
0.75
0.50
0.25
0.00
0
250
500
750
1000
1250
1500
1750
Frame

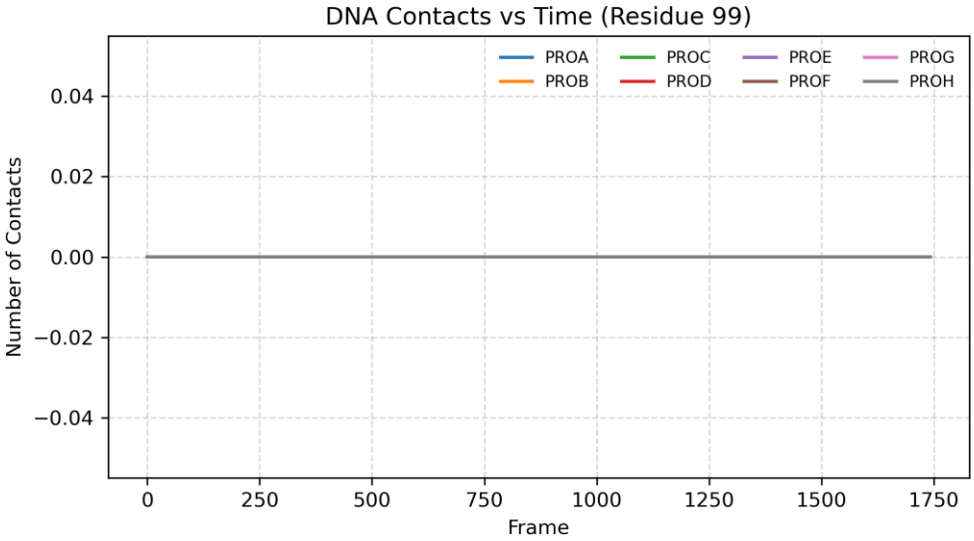
DNA Contacts vs Time (Residue 99)
PROA
PROB
PROC
PROD
PROE
PROF
PROG
PROH
Number of Contacts
0.04
0.02
0.00
−0.02
−0.04
0
250
500
750
1000
1250
1500
1750
Frame

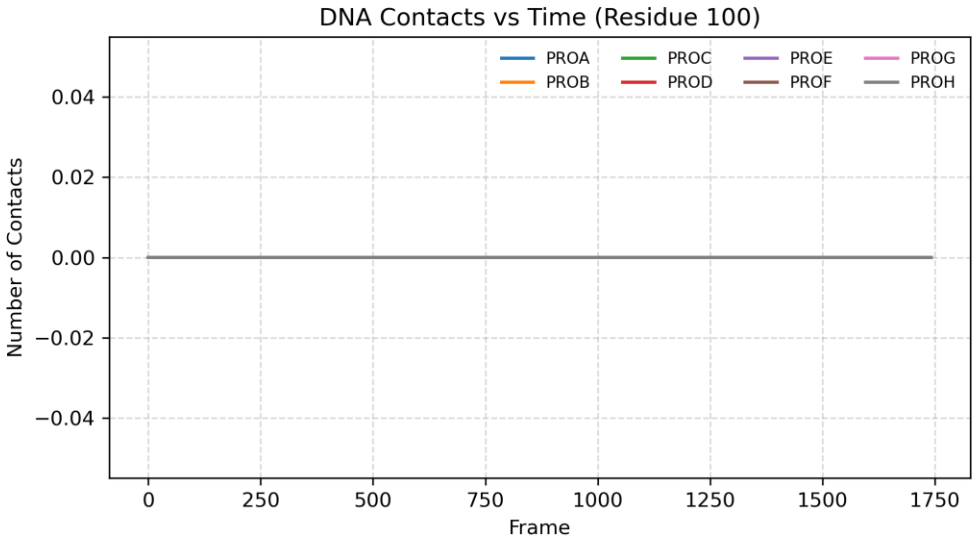
DNA Contacts vs Time (Residue 100)
PROA
PROB
PROC
PROD
PROE
PROF
PROG
PROH
Number of Contacts
0.04
0.02
0.00
−0.02
−0.04
0
250
500
750
1000
1250
1500
1750
Frame

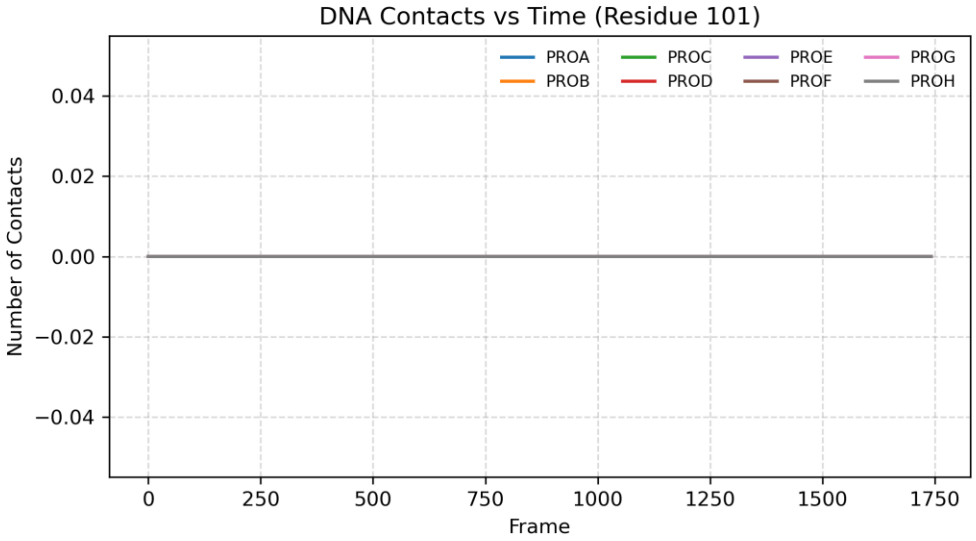
DNA Contacts vs Time (Residue 101)
PROA
PROB
PROC
PROD
PROE
PROF
PROG
PROH
Number of Contacts
0.04
0.02
0.00
−0.02
−0.04
0
250
500
750
1000
1250
1500
1750
Frame

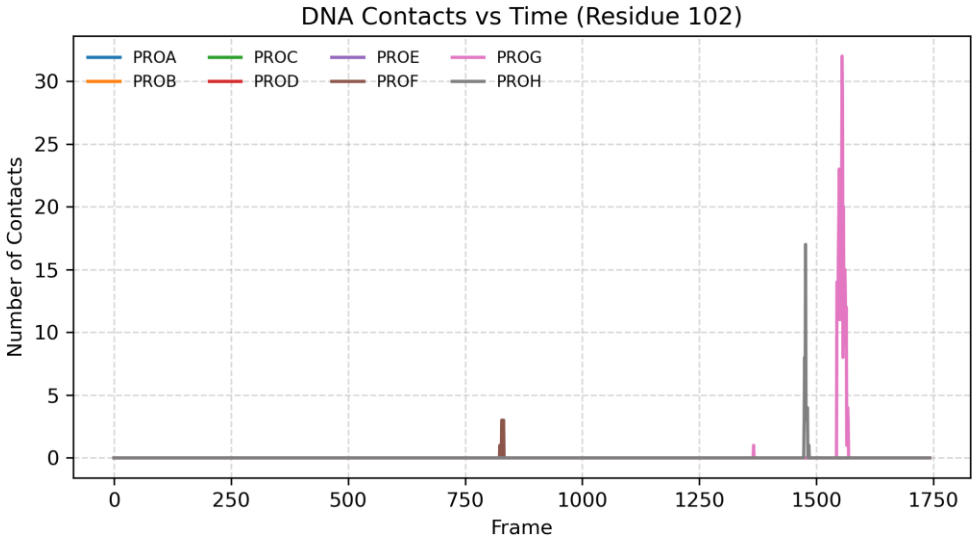
DNA Contacts vs Time (Residue 102)
PROA
PROB
PROC
PROD
PROE
PROF
PROG
PROH
Number of Contacts
30
25
20
15
10
5
0
0
250
500
750
1000
1250
1500
1750
Frame

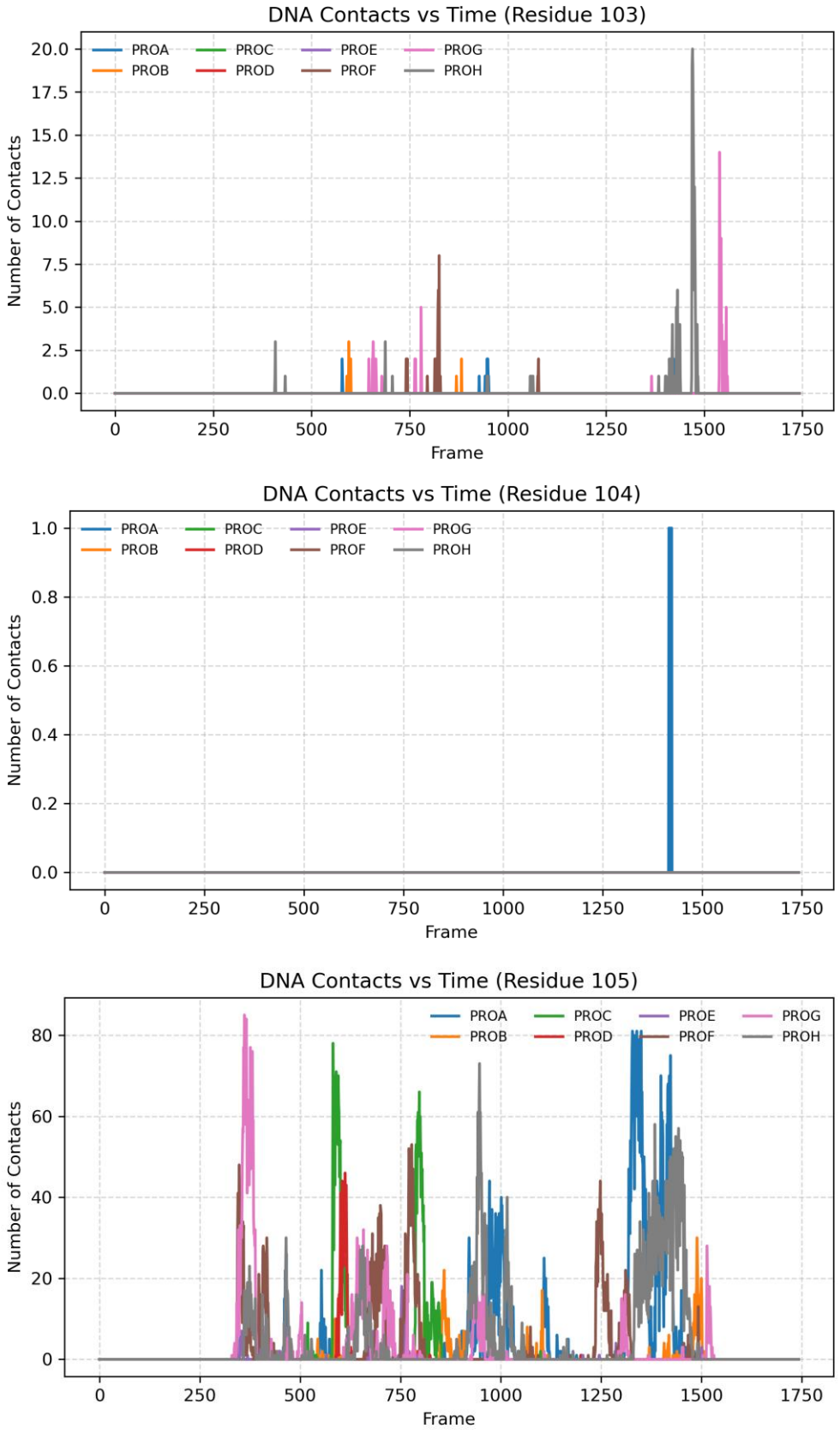

Figure S10: Residue wise contact formation between the residues of Pore exit of MSPA and the ssDNA.

S9. Snapshots of Residue locations in the Pore exit of MSPA forming Maximum contacts, Less contacts and no contacts:

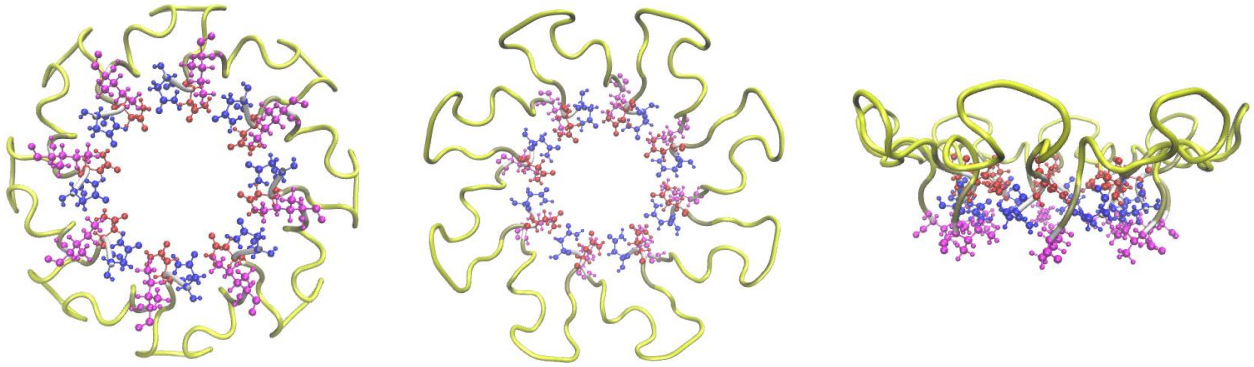

Figure S11: Top, bottom and side view snapshots of the location residues 90 (blue), 91 (red), 105 (magenta), forming maximum contacts with the ssDNA

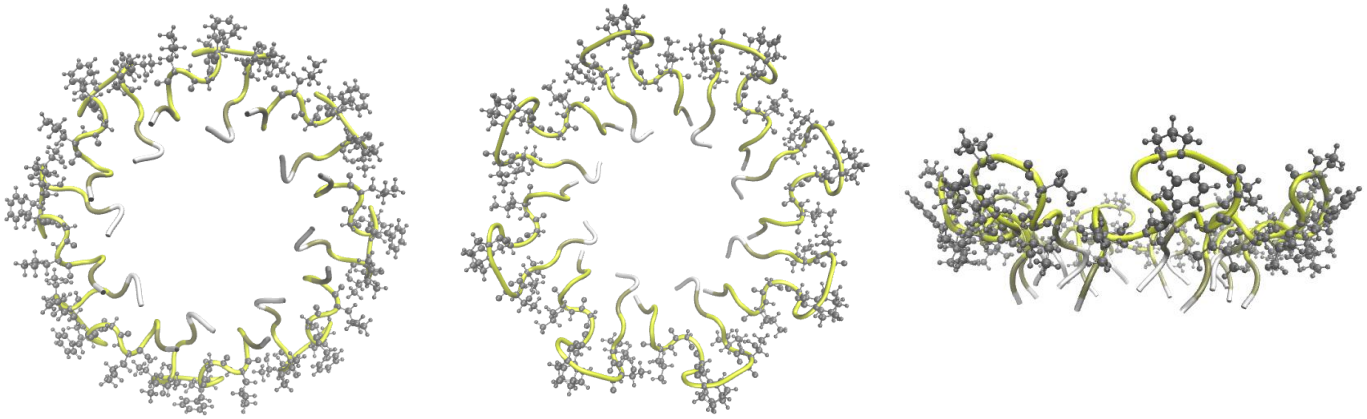

Figure S12: Top, bottom and side view snapshots of the location residues (showed in gray) 94, 95, 97, 99, 100, 101 forming no contacts with the ssDNA

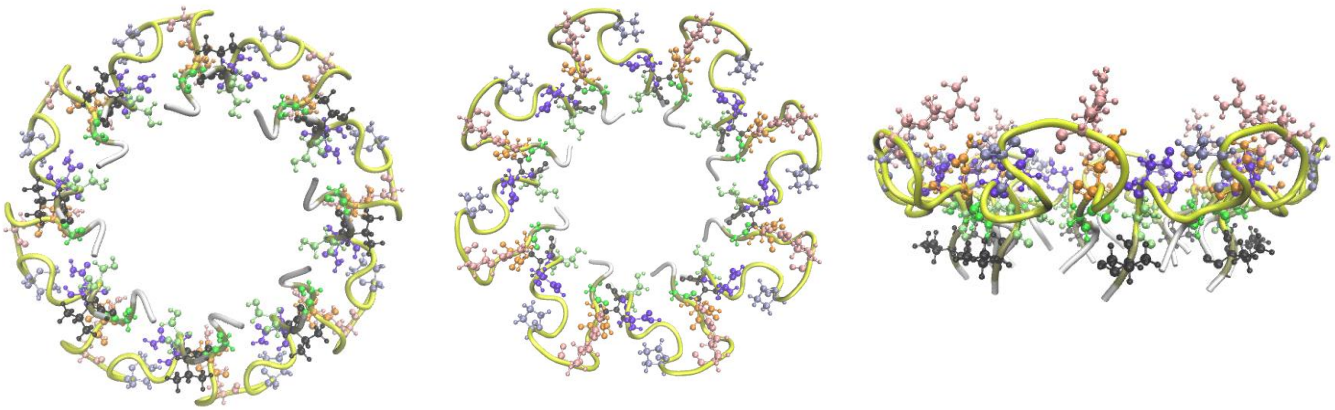

Figure S13: Top, bottom and side view snapshots of the location residues 92 (green), 93 (orange), 96 (pink), 98 (ice blue), 102 (violet), 103 (lime), 104 (black) forming few contacts with the ssDNA.

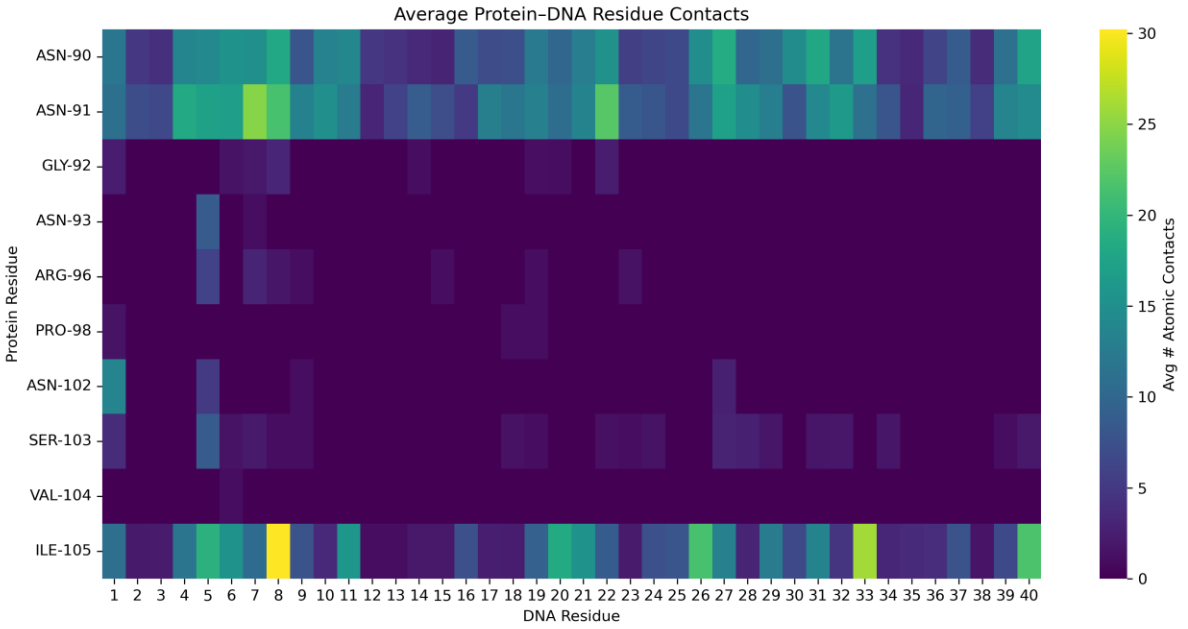

Figure S14: Residue-resolved contact heatmap between MSPA pore residues and ssDNA.

Heatmap showing the frequency of contacts between individual MSPA pore-lining residues and the translocating ssDNA, calculated over the production molecular dynamics trajectories. Residues are ordered according to their spatial location along the pore axis. The heatmap highlights distinct interaction hotspots at the pore exit, revealing residues that form persistent, transient, or negligible contacts with ssDNA during translocation.

S10. Atomic Decomposition of Residue-wise Contact formation between the Pore Exit residues and the ssDNA

The twofold characterization of pore-exit residue–ssDNA contacts reveals that polar atoms from polar and charged residues—such as the ND and OD atoms of asparagine and the NH atoms of arginine—as well as nonpolar atoms from hydrophobic residues, including the CD atoms of isoleucine, contribute significantly to ssDNA contact formation. These interactions collectively facilitate the association with the negatively charged ssDNA during translocation.

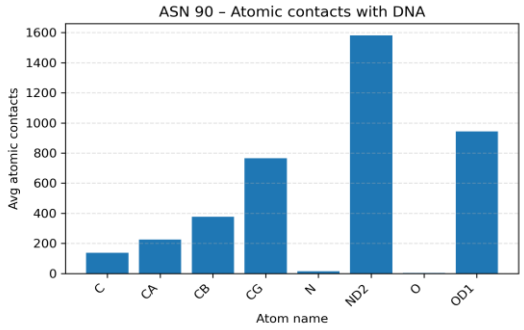

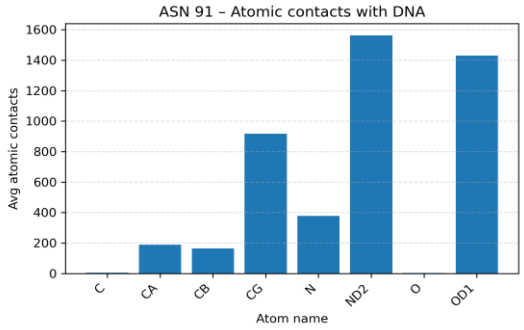

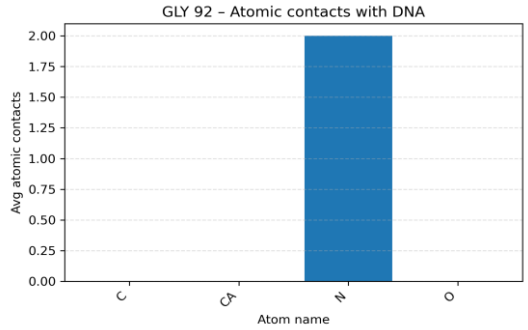

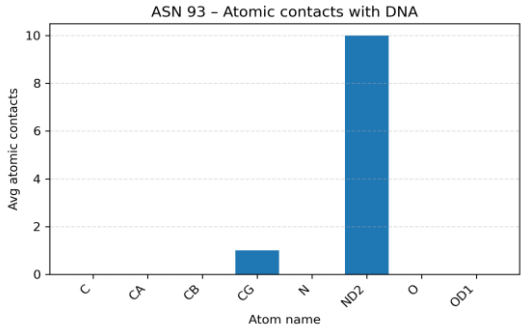

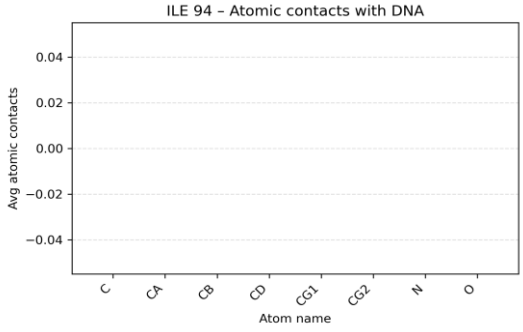

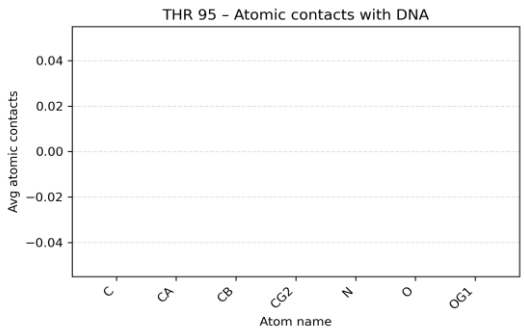

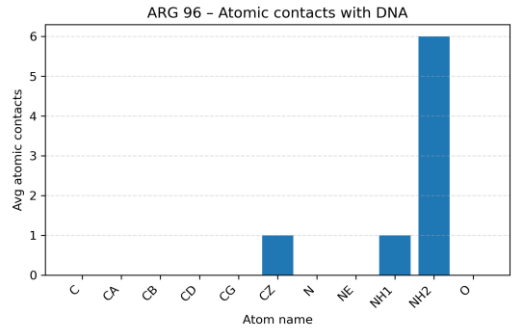
ARG 96 – Atomic contacts with DNA
Avg atomic contacts
Atom name
C
CA
CB
CD
CG
CZ
N
NE
NH1
NH2
O

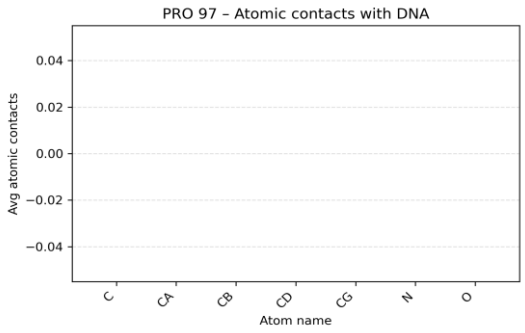
PRO 97 – Atomic contacts with DNA
Avg atomic contacts
Atom name
C
CA
CB
CD
CG
N
O

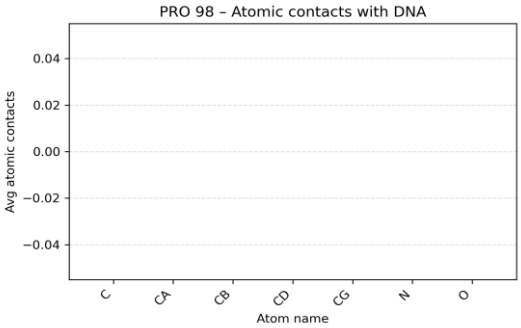
PRO 98 – Atomic contacts with DNA
Avg atomic contacts
Atom name
C
CA
CB
CD
CG
N
O

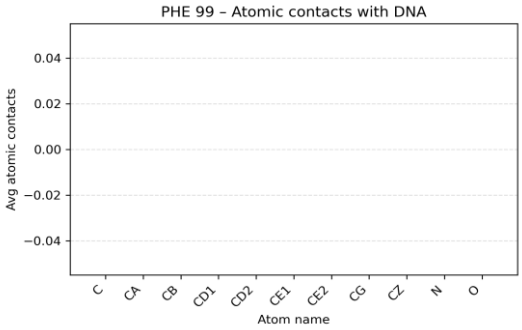
PHE 99 – Atomic contacts with DNA
Avg atomic contacts
Atom name
C
CA
CB
CD1
CD2
CE1
CE2
CG
CZ
N
O

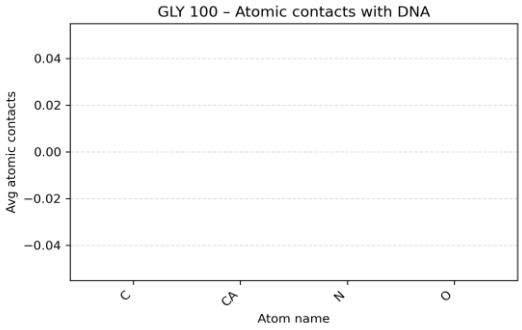
GLY 100 – Atomic contacts with DNA
Avg atomic contacts
Atom name
C
CA
N
O

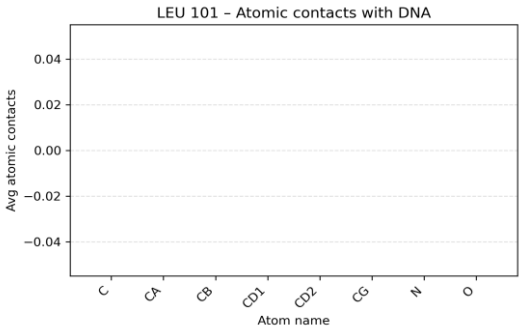
LEU 101 – Atomic contacts with DNA
Avg atomic contacts
Atom name
C
CA
CB
CD1
CD2
CG
N
O

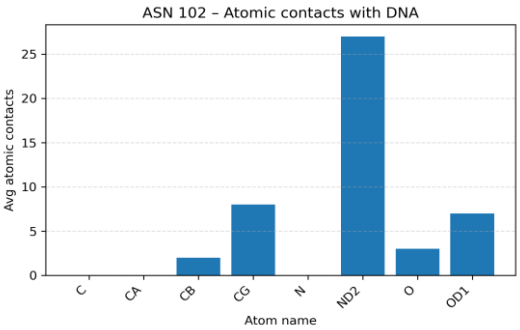
ASN 102 – Atomic contacts with DNA
Avg atomic contacts
Atom name
C
CA
CB
CG
N
ND2
O
OD1

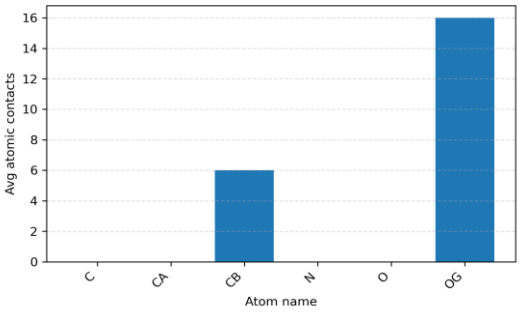
SER 103 – Atomic contacts with DNA
Avg atomic contacts
Atom name
C
CA
CB
N
O
OG

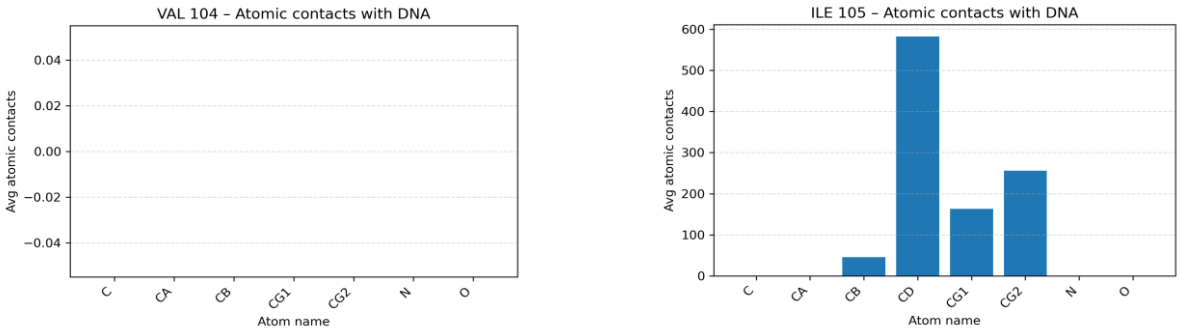

Figure S15: Plots for atomic decomposition of residue-wise contact formation between the pore exit residues and the ssDNA.

S11. Average Residue-wise Electrostatic Interaction between the MSPA Pore exit residues and the ssDNA

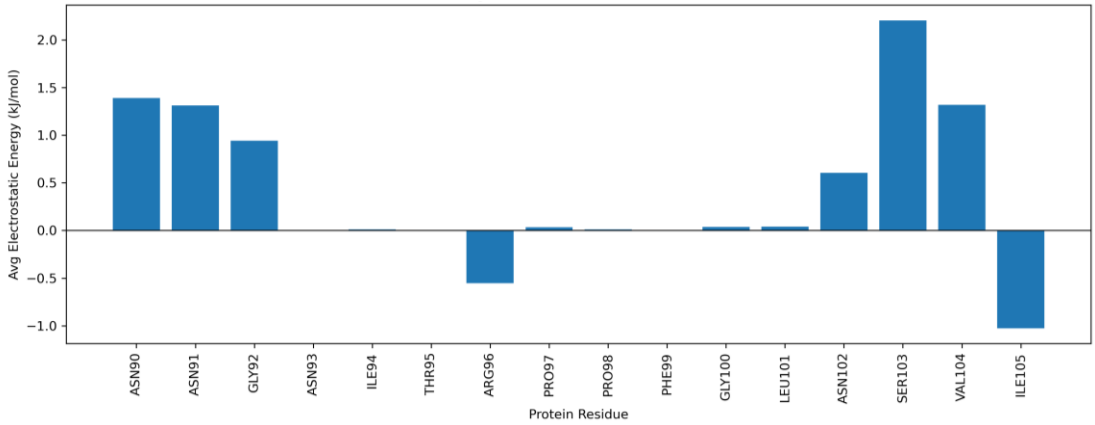

Figure S16: Electrostatic interaction energy between the pore exit residues and the ssDNA

The bar plot shows the overall average electrostatic interaction energy between individual MSPA pore-exit residues and ssDNA. Positively contributing residues (e.g., ASN90, ASN91, GLY92, SER103, VAL104) indicate favorable electrostatic interactions with the negatively charged ssDNA, whereas negatively contributing residues (e.g., ARG96, ILE105) reflect weaker or repulsive interactions. Residues with near-zero values exhibit minimal electrostatic involvement. The residue-specific electrostatic interaction profile at the pore exit plays a key role in facilitating ssDNA translocation through the MSPA nanopore. Favorable electrostatic interactions between positively charged or polar residues and the negatively charged phosphate backbone of ssDNA transiently stabilize the polymer as it passes through the pore, reducing energetic barriers and guiding its directional movement. At the same time, the presence of weakly interacting or repulsive residues prevents excessive binding, thereby avoiding kinetic trapping of ssDNA within the pore. This balance between stabilizing and destabilizing interactions promotes efficient, processive translocation by enabling controlled dwell times and smooth passage of ssDNA through the nanopore.

S12. Residue-wise Root Mean Square Deviation of the Pore Exit Residues (90-105): The residue-wise RMSD profile indicates that residues 94–98, which are located at the bottom-most region of the MSPA pore exit, exhibit relatively higher RMSD values, reflecting enhanced local flexibility. In contrast, the remaining pore-exit residues display lower RMSD values, indicating a more rigid and structurally stable environment. This localized flexibility at the pore bottom likely facilitates transient accommodation and release of ssDNA during translocation, while the surrounding rigid framework preserves overall pore integrity.

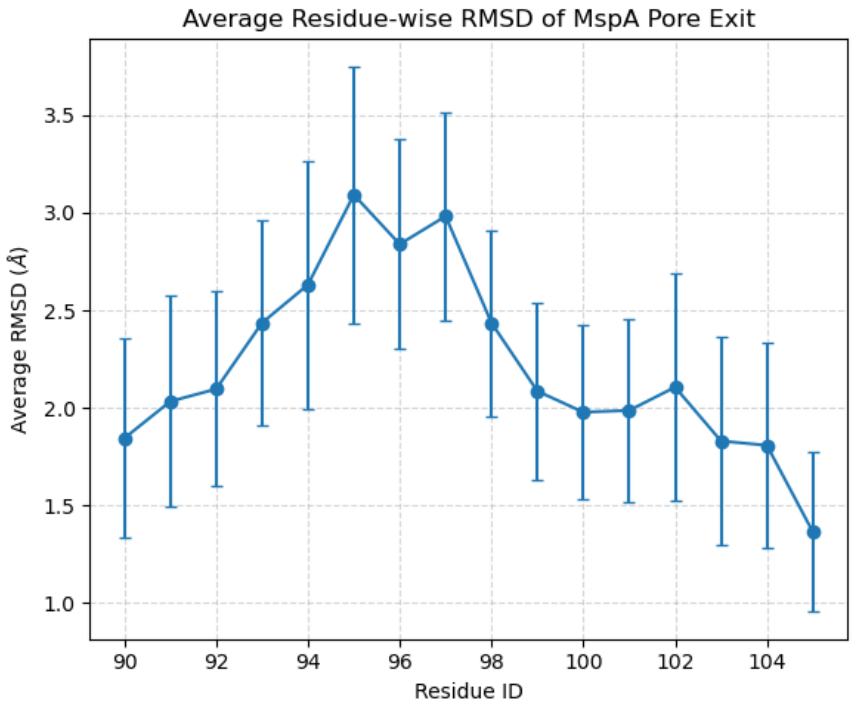

Figure S17: Average residue-wise RMSD of MSPA pore-exit residues

S13. Pore Size Analysis:

The mean pore radius was calculated along the simulation trajectories to assess the structural stability of the pore entrance during ssDNA translocation. The pore radius remains largely constant over time, indicating that the entrance maintains a stable geometry throughout the simulations.

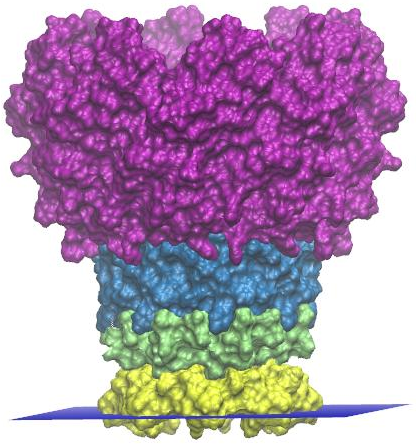

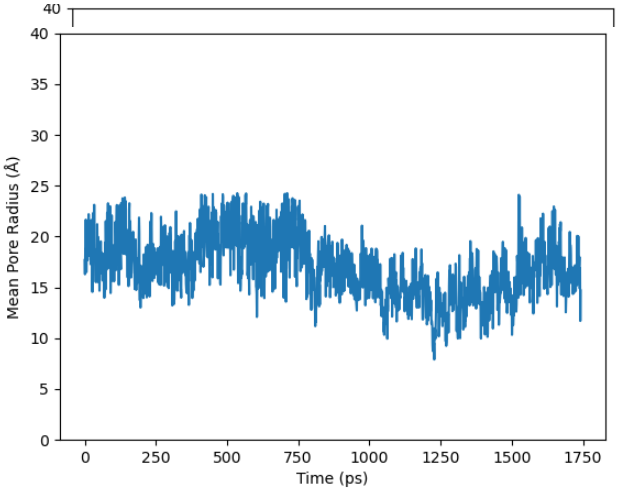

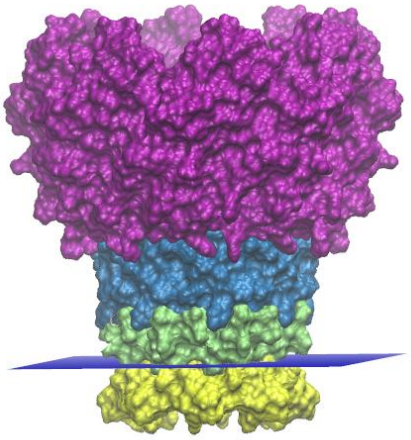

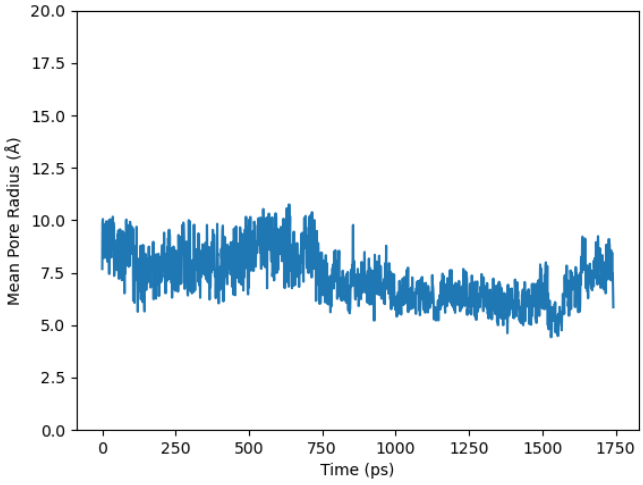

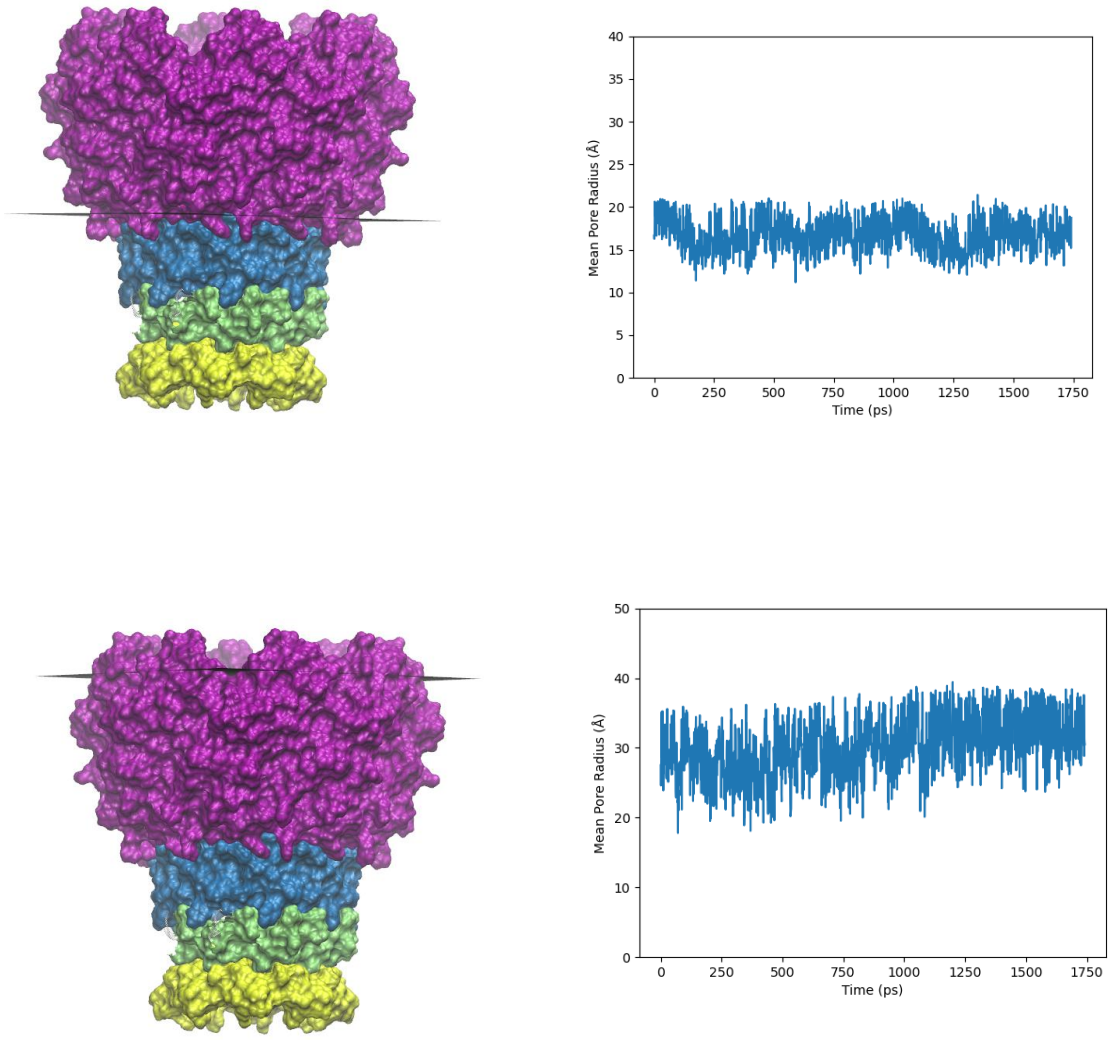

Figure S18: Temporal evolution of the mean pore radius at the MSPA pore parts.